

# Optical Properties of Tissue-like Phantoms

KESHAV SINGH

Submitted in partial fulfilment of the academic requirements of  
Master of Science

Physics  
School of Chemistry and Physics  
College of Agriculture, Engineering and Science  
University of KwaZulu-Natal  
Pietermaritzburg  
South Africa

07 February 2016

## PREFACE

The research contained in this thesis was completed by the candidate while based in the Discipline of Physics, School of Chemistry and Physics of the College of Agriculture, Engineering and Science, University of KwaZulu-Natal, Pietermaritzburg Campus, South Africa. The research was financially supported by the National Research Foundation (NRF).

The contents of this work have not been submitted in any form to another university and, except where the work of others is acknowledged in the text, the results reported are due to investigations by the candidate.

-----  
Signed: Dr N. Chetty (Supervisor)

Date:

-----  
Signed: K. Singh (Student)

Date:

## Declaration: Plagiarism

I, Keshav Singh, declare that:

- i. the research reported in this dissertation, except where otherwise indicated or acknowledged, is my original work;
- ii. this dissertation has not been submitted in full or in part for any degree or examination to any other university;
- iii. this dissertation does not contain other persons' data, pictures, graphs or other information, unless specifically acknowledged as being sourced from other persons;
- iv. this dissertation does not contain other persons' writing, unless specifically acknowledged as being sourced from other researchers. Where other written sources have been quoted, then:
  - (a) their words have been re-written but the general information attributed to them has been referenced;
  - (b) where their exact words have been used, their writing has been placed inside quotation marks, and referenced;
- v. where I have used material for which publications followed, I have indicated in detail my role in the work;
- vi. this dissertation is primarily a collection of material, prepared by myself, published as journal articles or presented as a poster and oral presentations at conferences. In some cases, additional material has been included;
- vii. this dissertation does not contain text, graphics or tables copied and pasted from the Internet, unless specifically acknowledged, and the source being detailed in the dissertation and in the References sections.

-----  
Signed: Keshav Singh

Date:

## Acknowledgements

The financial assistance of the National Research Foundation (NRF) towards this research is hereby acknowledged. Opinions expressed and conclusions arrived at, are those of the author and are not necessarily to be attributed to the NRF.

A few other acknowledgements deserve mention, to those people who gave me support through the duration of this dissertation and beyond.

- My friends and family who made this period a significantly more enjoyable and bearable one
- Staff of the physics and electronics departments from UKZN PMB for assistance with working space, equipment and their general encouragement, among others
  - Mr Ravin Sivraman
  - Mr Karl Penzhorn
  - Dr Vincent Couling
  - My Guy Dewar
- Mr Shawn Ball from chemistry stores for supplying me with some of the materials and equipment I needed to get the lab up and running
- My supervisor, Dr Naven Chetty for his patience and guidance through the duration of this work and ensuring the highest standard was maintained throughout
- Most of all, to my beautiful wife Herusha for her immense love, tireless support and endless motivation. The prospect of completing this work would have seemed ever more daunting if not for her.

## Abstract

This work involved the creation of optical phantom samples in an attempt to simulate the optical properties of human tissue. The experimental setup was designed to be as cost-effective as possible whilst remaining rigorous and reliable. The low cost design of the experiment was chosen to allow for repeatability and ease of use, making it applicable for any biomedical purposes in which minimal funding or equipment is available. Black ink was used as an absorber and  $\text{Al}_2\text{O}_3$  powder was used as a scatterer of visible light, both of which were mixed in varying quantities into a gel agar matrix. The ink dissolved evenly throughout the sample while the  $\text{Al}_2\text{O}_3$  particles were suspended in solution when the agar solidified. A He-Ne laser of wavelength 533 nm was incident upon different samples of phantoms and the incident and transmitted powers of light were measured to determine the attenuation in the sample. Measurements were made with slices of different thicknesses of the samples to determine the absorption coefficient  $\mu_a$ , scattering coefficient  $\mu_s$ , optical albedo  $a$  as well as the penetration depth  $\delta$  of light at this wavelength through each sample. The measurements of these optical properties were then compared to others that have been found by various authors in the literature. The results obtained show a close correlation between absorption effects of the samples created in this work and those of certain human tissues, eg. grey and white matter in the brain. Knowledge of these optical properties and their correlation to the appropriate human tissue can allow for the development of techniques in diagnostic and therapeutic applications of biomedicine. Some of these applications include, but are not limited to, laser ablation and PDT for cancer treatment.

# Contents

<b>1</b>	<b>Introduction</b>	<b>1</b>
<b>2</b>	<b>Theory</b>	<b>4</b>
2.1	Important Properties of Light . . . . .	4
2.2	Transmittance, Absorptance and Reflectance . . . . .	6
	2.2.0.1 Overview . . . . .	6
	2.2.0.2 Measurement of Transmittance . . . . .	6
	2.2.0.3 Measurement of Absorptance . . . . .	7
	2.2.0.4 Measurement of Reflectance . . . . .	7
2.2.1	Absorption Cross-section . . . . .	8
2.2.2	Scattering Cross-section . . . . .	10
2.3	Scattering by Particles . . . . .	11
	2.3.1 Overview . . . . .	11
	2.3.2 Single Scattering . . . . .	12
	2.3.3 Computational Methods . . . . .	15
	2.3.4 Multiple Scattering . . . . .	16
	2.3.5 The Radiative Transfer Equation . . . . .	17
2.4	Beer-Lambert Law . . . . .	18
2.5	Light and Lasers in Biological Systems . . . . .	20
	2.5.1 Overview . . . . .	20

2.5.2	Characteristics and Properties of Biological Tissue . . .	20
2.5.3	Light-Tissue Interactions . . . . .	22
2.5.3.1	Propagation of Light in Tissue . . . . .	22
2.5.3.2	Attenuation of Light . . . . .	26
2.5.4	Photodynamic Therapy (PDT) . . . . .	27
2.5.4.1	Lasers in Cancer Treatment . . . . .	27
2.5.4.2	Overview of PDT . . . . .	28
2.5.4.3	Mechanisms of PDT . . . . .	29
2.5.4.4	Photosensitisers . . . . .	30
2.5.4.5	Light . . . . .	31
2.5.4.6	Action of PDT . . . . .	31
2.5.5	Measurement of Optical Properties of Tissue . . . . .	32
2.6	Tissue Phantoms . . . . .	36
2.6.1	Overview . . . . .	36
2.6.2	Discrete and Continuous Particle Models of Tissue . .	38
2.6.2.1	Overview . . . . .	38
2.6.2.2	Distribution of Scatterers . . . . .	39
2.6.2.3	Absorption and Refractive Index . . . . .	39
2.6.2.4	Tissue Anisotropy . . . . .	40
2.6.2.5	Volume Fraction of Tissue Components . . . .	40
2.6.3	Construction of Tissue Phantoms . . . . .	41
2.6.3.1	Overview . . . . .	41
2.6.3.2	Host Media . . . . .	43
2.6.3.3	Scattering Media . . . . .	43
2.6.3.4	Absorbing Media . . . . .	44

<b>3</b>	<b>Experimental Details</b>	<b>45</b>
3.1	Methodology . . . . .	45
3.1.1	Apparatus . . . . .	45
3.1.2	Phantom Recipe . . . . .	46
3.1.3	Procedure . . . . .	48
3.2	Results . . . . .	50
3.2.1	Measurements . . . . .	50
3.2.2	Analysis . . . . .	59
<b>4</b>	<b>Discussion</b>	<b>63</b>
<b>5</b>	<b>Conclusion</b>	<b>67</b>

# List of Figures

2.1	The structure of a spectrophotometer [6] . . . . .	5
2.2	Transmission of light through a homogeneous absorbing medium [6] . . . . .	9
2.3	The absorption cross-section of a spherical particle [6] . . . . .	9
2.4	Transmission of light through a homogeneous scattering medium [6] . . . . .	10
2.5	The scattering cross-section of a spherical particle [6] . . . . .	11
2.6	Scattering of unpolarized visible light by spheres of radii 0.01, 0.1 and 0.2 $\mu m$ [10] . . . . .	14
2.7	A diagram representing a sample of thickness $b$ used for the derivation of the Beer-Lambert law [9] . . . . .	18
2.8	The relative sizes of various tissue components [6] . . . . .	22
2.9	A graph of the optical albedo as a function of the scattering coefficient [16] . . . . .	25
2.10	Absorption coefficient of oxy- and deoxyhaemoglobin as a function of wavelength [15] . . . . .	27
2.11	The electronic states and mechanism of cell death in PDT [18]	30
2.12	Some of the current applications of PDT [19] . . . . .	32
2.13	Experimental setups for measuring the total attenuation through a tissue sample [16] . . . . .	34
2.14	Optical properties of white matter of the human brain in its native and coagulated state [16] . . . . .	36

3.1	A diagram of the setup of apparatus for this experiment . . .	45
3.2	A pure agar sample after solidification . . . . .	47
3.3	An agar sample, containing $\text{Al}_2\text{O}_3$ particles, which has been stirred sufficiently until cool (left) compared to one that has had sedimentation occurring (right) . . . . .	48
3.4	A complete phantom sample with black India ink and $\text{Al}_2\text{O}_3$ particles in the agar gel mixture . . . . .	50
3.5	Graph of $\ln\left(\frac{P}{P_0}\right)$ vs $L$ for a pure agar sample with the associated best fit curve . . . . .	57
3.6	Graph of $\ln\left(\frac{P}{P_0}\right)$ vs $L$ for a complete phantom sample with 5 ml of ink and 0.10 g of $\text{Al}_2\text{O}_3$ , with the associated best fit curve . . . . .	57
3.7	Graph of $\ln\left(\frac{P}{P_0}\right)$ vs $L$ for a complete phantom sample with 2.5 ml of ink and 0.10 g of $\text{Al}_2\text{O}_3$ , with the associated best fit curve . . . . .	58
3.8	Graphs of all three samples plotted on the same set of axes to observe the difference in attenuation between samples . . . . .	58

# List of Tables

3.1	Measurements of the incident and transmitted power of a 632.8 nm wavelength, collimated light source through a pure agar sample, made with 100 ml of water and 1.5 g of agar, to determine the scattering coefficient of agar at this wavelength . . .	51
3.2	Measurements of the incident and transmitted power through a pure agar sample made with 100 ml of water and 1.5 g of agar, using light of wavelength 532 nm, to determine the scattering coefficient of agar at this wavelength . . . . .	52
3.3	Measurements of the incident and transmitted power through an agar sample made with 200 ml of water, 3.0 g of agar and 5 ml (5.50 g) of black ink, using light of wavelength 532 nm, to determine the transport coefficient of ink in agar at this wavelength . . . . .	53
3.4	Measurements of the incident and transmitted power through an agar sample made with 200 ml of water, 3.0 g of agar and 2.5 ml (2.76 g) of black ink, using light of wavelength 532 nm, to determine the transport coefficient of ink in agar at this wavelength . . . . .	53
3.5	Measurements of the incident and transmitted power through an agar sample made with 200 ml of water, 3.0 g of agar and 0.1 g of $\text{Al}_2\text{O}_3$ , using light of wavelength 532 nm, to determine the transport coefficient of $\text{Al}_2\text{O}_3$ in agar at this wavelength . .	54

3.6	Measurements of the incident and transmitted power through a complete phantom sample made with 200 ml of water, 3.0 g of agar and 5 ml (5.51 g) of black ink, using light of wavelength 532 nm, to determine the transport coefficient of ink and $\text{Al}_2\text{O}_3$ in agar at this wavelength . . . . .	55
3.7	Measurements of the incident and transmitted power through a complete phantom sample made with 200 ml of water, 3.0 g of agar and 2.5 ml (2.75 g) of black ink, using light of wavelength 532 nm, to determine the transport coefficient of ink and $\text{Al}_2\text{O}_3$ in agar at this wavelength . . . . .	55
3.8	The transport coefficients and penetration depths for all the samples obtained by direct calculation . . . . .	59
3.9	The transport coefficients and penetration depths for all the samples obtained from Gnuplot . . . . .	60
4.1	Optical properties of human tissue (in vitro) from various sources	64

# Chapter 1

## Introduction

In the biomedical sciences, subdermal imaging is becoming ever more popular. This is due, in part, to significant progress in the development of lasers, fibre optics and other associated technologies [1]. The medical field requires relevant instrumentation to analyze biological systems. In the recent past, efforts have been made to use optical techniques such as Raman spectroscopy, fluorescence spectroscopy and elastic scattering spectroscopy for the early diagnosis and treatment of various diseases [1]. Optical imaging techniques such as coherence gated imaging [1], amongst others are also currently being employed for obtaining high resolution images of biological samples and their basic structure. For optical diagnosis, the property of light known as scattering is exploited; elastic and inelastic light scattering spectra from tissues are examined. This is carried out by the measurement of the intensity of light, as it propagates through dermal tissue into the subdermal layers of the skin. The scattered light contains useful biological and chemical information about the sample, which can be investigated, to determine if any biochemical anomalies are present. This could provide evidence of the progression of a certain disease [1]. The scattering of light through a biological sample is hence a possible tool for diagnosis of certain diseases, but this would require a model of light scattering in an appropriate complex medium, i.e. a simulator for human skin in this case [1].

The main advantage of imaging in the biomedical field is that it is non-invasive [1,2]. By observing the different wavelengths of light that can radiate through human dermal tissue, it is possible to generate a picture of subder-

mal layers of the skin and diagnose and cure certain skin conditions such as jaundice, erythema and even cancer [2]. Measurements of light intensity taken from different points on human skin tissue can indicate the penetration depth of a certain wavelength of light [3]. This in turn provides useful information about the wavelength of light needed for the diagnosis and safe, effective treatment of the underlying medical condition.

Biological tissues are optically inhomogeneous and absorbing with an average refractive index which is higher than that of air. Reflection occurs at the air-tissue boundary but a large fraction of the incident light passes through the tissue. Multiple scattering and absorption events occur as the light propagates through the tissue [4]. In the case of lasers, these properties of light are responsible for the broadening and eventual decay of the laser beam as it travels through a tissue. Light propagation within a tissue therefore depends on the scattering and absorption properties of its components such as cells, cell organelles, etc [4]. The shape of these components, their size, density and refractive index relative to the basic tissue substance all play important roles in the propagation of light in tissues. The complexity of a tissue requires a complex study into the creation of adequate models to simulate the optical properties, such as the scattering and absorption, of that tissue [4]. The approach being employed, in this work, for tissue modeling is to treat the modeled tissue as a medium with a random, continuous spatial distribution of scattering particles. The choice of this approach is convenient in terms of efficiency, cost and the nature of the scattering characteristics that were sought [4].

Tissues and other biological media can be modeled physically by a distribution of homogeneous spherical particles, since many cells, especially blood cells, are nearly spherical in shape. A system of spherical particles, which do not interact with each other, is the simplest tissue model. Mie theory is generally applied to describe the scattering of light due to a spherical particle, and can hence be applied to the model of a simple tissue [4]. The application of this model would have to take into account the structure of each spherical particle, the anisotropy, and optical activity. The sizes of basic tissue structures and cells can vary in size from the order of a few tenths of nanometers to hundreds of micrometres [4].

In this work optical phantom samples were created in an attempt to simulate the optical properties of human tissue. The experimental setup was designed to be as cost-effective as possible whilst remaining rigorous and reliable. A He-Ne laser of wavelength 533 nm was incident upon different samples of phantoms and the incident and transmitted powers of light were measured to determine the relevant optical characteristics of the phantoms, at this wavelength. Knowledge of these optical properties and their correlation to the appropriate human tissue can allow for the development of techniques in diagnostic and therapeutic applications of biomedicine. Some of these applications include, but are not limited to, laser ablation and PDT for cancer treatment [2].

# Chapter 2

## Theory

### 2.1 Important Properties of Light

Scattering, absorption, reflection and transmission are the most significant properties of light in the case of light propagation through biological systems, such as tissue. Transmission refers to the ability of light to pass through an object. An object that allows light to pass through is said to transmit the light incident on it. Certain objects do not completely transmit light but absorb some of the radiation, usually converting it to heat. This property is known as absorption. Generally, the thicker the material, the greater its absorption, i.e. less light is transmitted as the thickness of a material is increased. Reflection occurs when the light incident on a surface changes direction upon meeting the surface and propagates back into the medium from which it came, hence the term reflection [5]. Specular reflection occurs when the angle of incidence of the light is the same as the angle of reflection (i.e. the angle at which the light reflects off the surface). This is usually the case with smooth surfaces such as mirrors. When the surface is rough, the incident light tends to reflect or transmit in many different directions at once and this phenomenon is known as scattering (also known as diffusion) [5]. The amount of light being scattered when passing from one medium to another depends on the wavelength of the incident light and how this compares to the size of the particles in the second medium (biological tissue in the case of biomedical imaging). Scattering is also dependent on the difference in the refractive indices of the two media. These properties apply to visible light

and other forms of electromagnetic radiation [5].

Experimentally, spectrophotometers (Figure 2.1 [6]) are the instruments employed to measure reflectance and transmission of light incident on a surface. The readings from the spectrophotometer can be made more accurate by using an integrating sphere, to "diffuse" incident light [2]. The illuminance measured on the surface of the object is the same (with relatively small deviations) at all points on the object. Spectrophotometers can also be used to measure the absorption of light by an object [2].

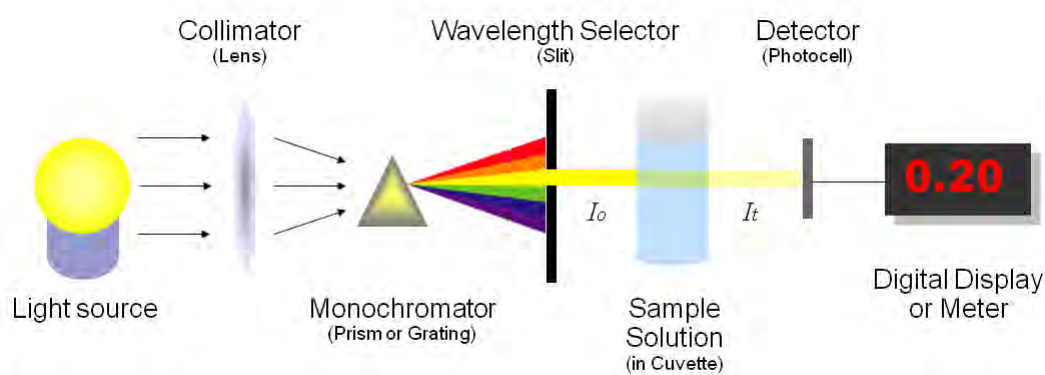


Figure 2.1: The structure of a spectrophotometer [6]

Biological tissue scatters light strongly in the forward direction [7]. For deeper, more effective penetration through skin, the incident light must lie within a wavelength range that is more likely to scatter than be absorbed by the skin. For visible light (such as He-Ne lasers) this range, in which the ratio between scattering and absorption is very high, is in the neighbourhood of 650nm [8]. Models such as Mie theory and the Born approximation have been used to describe the scattering of light through tissue more accurately [1]. Algorithms have also been written and transformed into code which is programmed to simulate the effects of light radiating through human tissue. Currently these methods are being used to understand the scattering and absorption of light in inhomogeneous media, such as tissue. This is clearly a difficult process as it requires most, if not all, inhomogeneities to be accounted for in the simulation.

## 2.2 Transmittance, Absorptance and Reflectance

### 2.2.0.1 Overview

The transmittance  $T$  of a medium is defined as the ratio of the transmitted intensity of light  $I_T$  to the incident intensity of light  $I_0$ , on that medium, i.e.

$$T = \frac{I_T}{I_0}. \quad (2.1)$$

Similarly, the absorptance  $A$  of a medium is the ratio of the absorbed intensity (or radiant flux)  $I_A$  to the incident intensity,

$$A = \frac{I_A}{I_0}. \quad (2.2)$$

The reflectance  $R$  of a medium is the ratio of the reflected intensity  $I_R$  to the incident intensity:

$$R = \frac{I_R}{I_0}. \quad (2.3)$$

For a material that absorbs a fraction of incident light whilst transmitting the rest, or vice versa

$$I_0 = I_T + I_A + I_R, \quad (2.4)$$

where  $I_A$ ,  $I_T$  and  $I_R$  are wavelength-dependent. Hence

$$T(\lambda) + R(\lambda) + A(\lambda) = 1. \quad (2.5)$$

### 2.2.0.2 Measurement of Transmittance

Understanding the transmission of light through optical materials, various gases and liquids is necessary to study the behaviour of the atmosphere, biological cells and many other natural phenomena. Spectrophotometers (Figure 2.1) can be susceptible to stray radiation, which allows for uncertainties in measuring samples that are highly absorbing in one region whilst transmitting in another. Conventional instruments are limited to uncertainties on the

order of about 0.1%. For lower uncertainties, the performance of the instrument is affected, however this can be overcome by a change in structure of the spectrophotometer [9].

The spectrometer can be set at a fixed wavelength and repeated measurements can be made whilst ensuring that the geometry of the beam remains the same. For the most accurate results, the beam being analysed should be highly collimated, as is the case with a conventional laser, stray light has to be minimised and an integrating sphere used to diffuse incident light and negate the effects of beam shifts. A calibrated spectrophotometer can also be utilised to determine linearity and to analyse stray light. Particular attention has to be paid to certain luminescent samples that absorb radiant energy in one spectral region and re-emit it at longer wavelengths [9].

### **2.2.0.3 Measurement of Absorptance**

Usually absorptance is not measured directly, but is inferred from the measurements of transmission, with appropriate corrections for reflection losses. These corrections can be calculated from the Fresnel equations if the index of refraction is known. If the material has a significantly small absorption, this method is not viable and in such a case, laser calorimetry measurements can be carried out to directly measure the absorptance [9].

### **2.2.0.4 Measurement of Reflectance**

Various instruments and methods can be applied for the measurement of reflectance (e.g mirror detection using reflectometers and averaging spheres) [9]. Characterising the appearance of any material involves measuring the specular and diffuse reflectances. Reflectometers employ the use of mirrors to measure absolute specular reflectance. Most measurements of diffuse reflectance involve the use of an integrating sphere which is the preferred instrument for measurements in the visible and near infrared spectral regions for both specular and diffuse materials. Integrating sphere measurements are normally made with reference to some standard, but an absolute reflectance can be determined via the doublesphere method. A perfect diffuse reflector is used to provide a white reflectance standard, to which relative reflectances

can be determined. Lasers and other coherent sources are employed to characterise smooth surfaces, i.e. specular reflection and incoherent sources, such as tungsten-halogen sources, are often used for more diffuse specimens [9].

### 2.2.1 Absorption Cross-section

Absorption by tissue can have either a therapeutic effect or a destructive one. Energy from incident waves is transferred to the tissue at each absorption event, and if no absorption occurs then there is no energy transfer between the incident radiation and the tissue. Absorption of light by tissue also plays a diagnostic role in tissue spectroscopy and medical imaging, amongst others. Absorption can only occur if the energy of the incoming photon  $h\nu$  is identical to the difference in energy between energy levels  $\Delta E$  in the molecule onto which radiation is incident, i.e.

$$\Delta E = h\nu. \tag{2.6}$$

As a result of the absorption, the molecule undergoes a quantised change in charge separation and a quantised change in its vibrational state.

Classically we can adopt the following formalism for absorption. Consider a collimated beam of light with wavelength  $\lambda$  and intensity  $I_0$  passing through a homogeneous medium with absorption coefficient  $\mu_a$  ( $\text{cm}^{-1}$ ). The light intensity  $I$  transmitted through the medium of width  $L$  is given by:

$$I = I_0 e^{-\mu_a L}, \tag{2.7}$$

where  $L$  is also known as the photon path length. Figure 2.2 [6] illustrates this concept.

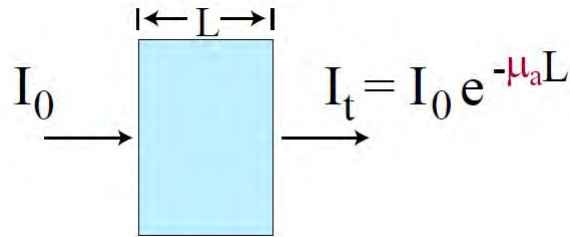


Figure 2.2: Transmission of light through a homogeneous absorbing medium [6]

The absorption coefficient can also be expressed as

$$\mu_a = \rho_a \sigma_a, \quad (2.8)$$

in which  $\sigma_a$  is known as the absorption cross section ( $\text{cm}^2$ ) and  $\rho_a$  is the particle number density of the absorbers in the medium. By definition:

$$\sigma_a = Q_a A, \quad (2.9)$$

where  $Q_a$  is the absorption efficiency and  $A$  is the geometrical area of the absorbing particle. We can approximate the absorbing particle to ideally be a sphere, as shown in Figure 2.3 [6]

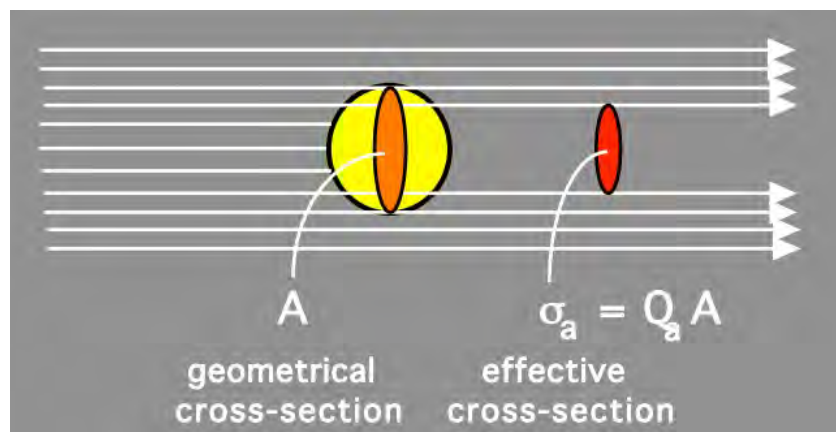


Figure 2.3: The absorption cross-section of a spherical particle [6]

## 2.2.2 Scattering Cross-section

Similarly, for scattering we take the same considerations into account and we have

$$I = I_0 e^{-\mu_s L}, \quad (2.10)$$

where  $L$  is again the photon path length.

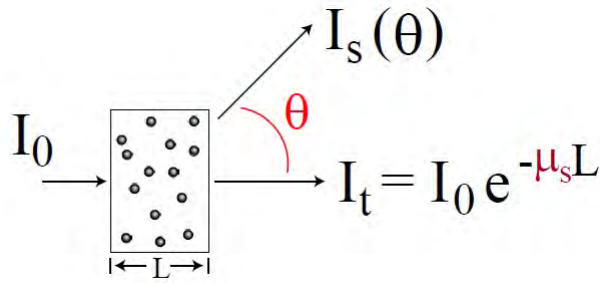


Figure 2.4: Transmission of light through a homogeneous scattering medium [6]

Analogously, the scattering coefficient (Figure 2.4 [6]) can also be expressed as:

$$\mu_s = \rho_s \sigma_s, \quad (2.11)$$

where  $\sigma_s$  is the scattering cross section ( $\text{cm}^2$ ) and  $\rho_s$  is the particle number density of the scatterers in the medium. By definition

$$\sigma_a = Q_a A, \quad (2.12)$$

and  $Q_s$  is the scattering efficiency with  $A$  being the geometrical area of the scattering particle, as illustrated in Figure 2.5 [6].

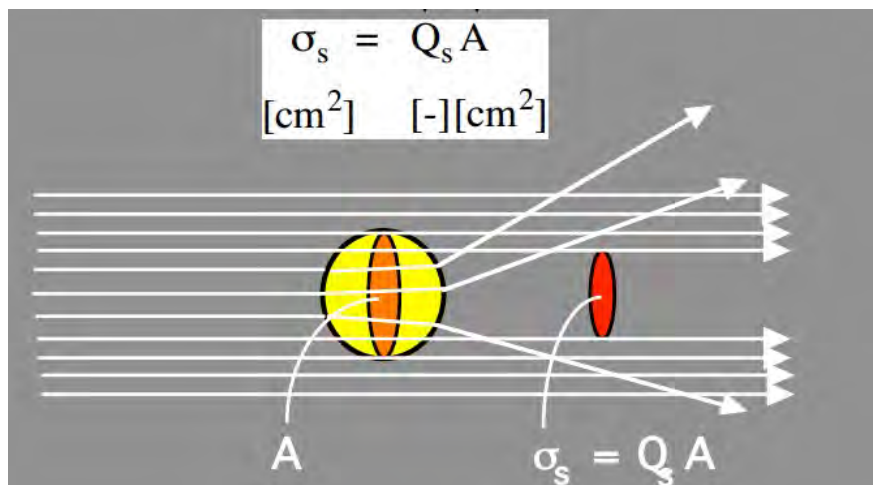


Figure 2.5: The scattering cross-section of a spherical particle [6]

## 2.3 Scattering by Particles

### 2.3.1 Overview

Scattering by particles can be treated by classical electromagnetic theory (as will be the case in this work). Matter is often electrically neutral, however it is still composed of multiple discrete charges. Since light is an oscillating electromagnetic field, it can excite the charges in matter and cause them to oscillate. These oscillating charges then radiate electromagnetic waves which are the scattered (secondary) waves. The superposition of the scattered waves with the incident waves is observed. Elastic scattering (coherent scattering) occurs if the frequency of secondary waves is approximately the same as the frequency of the source [10].

It has long been assumed that specular reflection occurs at "smooth" surfaces, however the smoothest of surfaces are in fact quite irregular on the scale of a photon. If photons are considered as tiny particles, they should be scattered in all directions by a surface such as this. The notion of the angles of incidence and refraction also become difficult to define in this situation [10]. Approaching this situation geometrically satisfies what is observed as well as

the fact that reflected and refracted fields satisfy the Maxwell equations. One interpretation of scattering describes the reflected and refracted waves as the superpositions of scattered secondary waves induced by the incident wave [10]. Thus, reflected and refracted light are just forms of scattered light. This gives rise to an important concept in the understanding of light, i.e. there is no fundamental distinction between specular reflection, refraction, diffraction and scattering by particles. All occur by the interaction of light with matter, only differing in their geometries and the theories used to describe them. [10]

### 2.3.2 Single Scattering

Analysis of light scattered by particles was found to be useful in many areas of science from astronomy to cell biology and even atmospheric science [10]. Molecules can scatter light but are not treated as particles [10]. The study of scattering by particles is generally approached by the wave definition of light, however multiple scattering by many particles can be dealt with by applying the photon nature of light. It is far simpler to estimate single scattering events in theory than it is in practice, as multiple scattering is more frequently observed experimentally. Single scattering can only be observed by an individual, isolated scattering particle upon which radiation from a certain source is incident [10].

Scattering can be treated as occurring due to regular (coherent) or irregular array of particles. For scattering by a coherent array of particles, (e.g. pure water molecules) the wave nature of the incident light is prominent and phases must be accounted for, whereas in scattering by irregular (incoherent) arrays (e.g. blood cells in tissue), the phases may be ignored. Incoherent arrays are normally more likely to scatter light in all directions whilst coherent arrays will weakly scatter light as most of the light is reflected or refracted. Multiple scattering is possible in both types of arrays, and cannot be neglected nor is it a simple scaling up of a single scattering event and this becomes apparent when observed experimentally [10].

Scattering by single particles is induced by the arrangement of the dipoles that radiate (scatter) an incident oscillating electric field. The factors which determine the degree of scattering include the shape and size of the scattering particle, the angle (geometry), polarization state and frequency of the

incident radiation. The total power/intensity of incident radiation scattered by a particle is determined by the scattering cross-section of the particle  $\sigma_s$ , and similarly the total power absorbed by the particle is determined by the absorption cross-section  $\sigma_a$  [10]. The sum of these gives the extinction cross-section

$$\sigma_{ext} = \sigma_s + \sigma_a. \quad (2.13)$$

For this result we have assumed that the incident radiation is relatively large (higher wavelength) in size in comparison with the size of the particle, satisfied by the idea of plane waves, which is generally the source of incident light in scattering experiments. To determine the extinction cross-section, measurements of transmission of radiation through a slab of  $N$  identical scattering particles per unit volume can be carried out. The relationship between the incident radiation and the transmitted radiation is given by

$$I(h) = I_0 e^{-N\sigma_{ext}L}, \quad (2.14)$$

where  $L$  is the thickness of the slab and provided that multiple scattering is negligible [10]. These transmission measurements yield the extinction coefficients only and to obtain separate absorption and scattering cross-sections, additional measurements have to be carried out. Equation (2.14) requires that all particles in the slab be identical and to account for the generalized form in which there are differences between particles,  $N\sigma_{ext}$  is replaced by

$$\sum_j N_j \sigma_{ext,j},$$

where  $j$  denotes all parameters distinguishing one particle from another [10].

The following graph (Figure 2.6) [10] indicates the amount of scattering produced by particles of different radii, using the Rayleigh-Gans approximation.

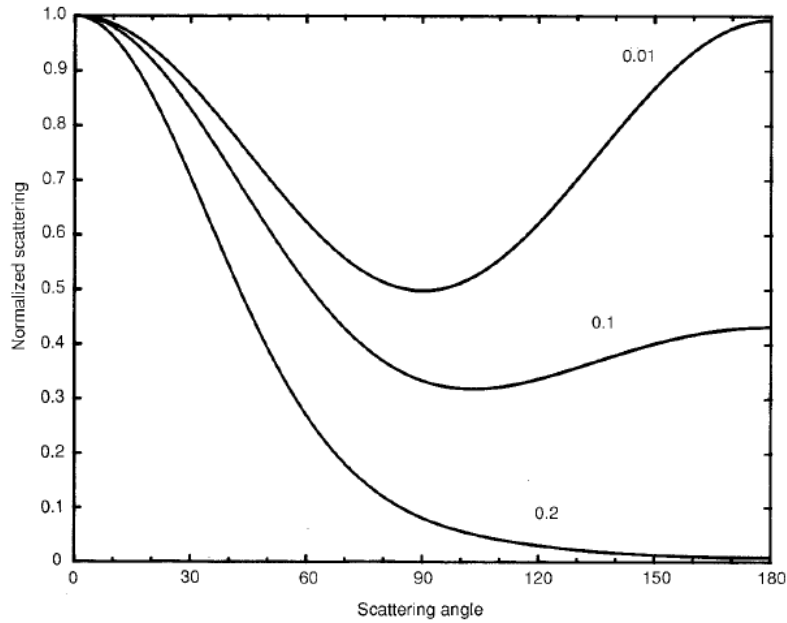


Figure 2.6: Scattering of unpolarized visible light by spheres of radii 0.01, 0.1 and 0.2  $\mu m$  [10]

It is clear from this that a small sphere, even of the order 0.2  $\mu m$ , can scatter light strongly in the forward direction.

The simplest particle to consider, from which scattering theories can be defined, is an isotropic, homogeneous sphere. There are many theories and models to describe the scattering of light, such as Rayleigh and Mie theories. One of the most applied theories, Mie theory (from Gustav Mie), describes the scattering of radiation due to these spherical particles that are the same size or much larger than the wavelength of incident radiation. Rayleigh theory is included in Mie theory, but applies only as the size of the scatterers approaches zero. Hence a particle can be either a Rayleigh or a Mie scatterer depending on the wavelength of the illuminating radiation. Mie theory works well when applied to single spherical particles but starts to break down when used in cases of irregularly shaped particles or in the instance of scattering by molecules. It also is better suited for use when computing forward scattering rather than backscattering, which makes it the preferred theory for use in tissue optics. Ricatti-Bessel functions are utilised in Mie theory to

describe the scattering by spherical particles and were once worked on rigorously by mathematicians, however these expressions and equations can be easily solved in minutes by a modern computer. Algorithms applying Mie theory can be written and coded to simulate all the relevant characteristics of scattering events [10].

Any particle that is spherically symmetric induces a scattered field of the same form as that of a homogeneous sphere, all that differs are the scattering coefficients. Different spherically symmetrical particles include uniformly coated spheres and multilayered spheres. These particles can be modelled using Bessel functions to describe their absorbing/scattering properties. Uncoated spheres are easier to work with computationally as they scatter strongly and are weak absorbers or non-absorbing, whereas coated spheres absorb strongly, making the mathematics more complicated [10].

The treatment of scattering by spheres and circular cylinders is fairly similar, with related Bessel functions. However, an infinitely long cylinder cannot have a finite volume and hence the field scattered differs to that of a finite sphere. There is no exact theory that exists for the treatment of scattering by finite cylinders, but approximations can be made by neglecting the end effects of cylinders which have a large ratio of their length to diameter (aspect ratio). The geometry of the situation differs between the sphere and cylinder, in that the scattering for cylinders depends on the polarization of the incident plane wave. The orientation of the incident waves scattering off a cylindrical particle determines the polarization state of the excited/scattered wave. As with spheres, the coated cylinder presents more of a challenge to work with than the uncoated cylinder as the Bessel functions can have values which are out of most computational bounds [10].

### 2.3.3 Computational Methods

Spherical particles are less common than nonspherical, irregular particles. This indicates that it is difficult to readily apply Mie theory in a physical situation, and other methods have to be used to coincide with what is observed in reality. These methods are all, in some way, linked by the elementary Maxwell's equations. One method, known as the T-matrix method is based

on the scattering by a single, arbitrary particle, and is an integral representation of scattering by single particles. The field and boundary conditions of the incident wave being linear imply that the scattered field shares a linear relationship with the incident field. The linear transformation that links these two sets of coefficients is called the T-matrix, the elements of which are found by numerical integration. Difficulties arise with the computation when working with particles which are highly absorbing or have a large aspect ratio. These prove to be some of the limitations of the T-matrix method, along with the fact that it is a complex method to understand. The Purcell-Pennypacker method is a computational application of the Green's function and is easier to work with mathematically than the T-matrix method. A particle is approximated by a lattice of  $N$ , often identical and isotropic, dipoles each small compared to the wavelength of incident radiation. The dipoles are excited by the incident field and the fields of all the other dipoles, thus leaving a set of  $3N$  linear equations at each dipole. The  $3N \times 3N$  coefficient matrix can be inverted and used to calculate scattering for various orientations. This method is limited in that the amount of storage used by the computer can be excessive [10].

### 2.3.4 Multiple Scattering

In nature, it is far more likely for electromagnetic waves to be scattered by many particles when incident upon a surface, rather than a single scatterer. Waves that pass through media which contain a large amount of discrete scatterers will undergo many scattering events, which makes the wave equation difficult to solve. Various techniques can be applied to account for these multiple scattering events.

A medium can be considered as a random distribution of single spheres, in which the attenuation due to scattering is negligible, provided the incident wavelength is much larger than the size of the scattering particles and the mean separation between scatterers. A frequency-dependent dielectric constant can, in this situation, describe the medium.

T-matrices and Green's functions can be used to approximate multiple scattering processes, but in cases for large ensembles of scattering particles probability density functions are used to determine the locations of individual

scattering centres. Integral equations can also be set up to describe the field as it fluctuates through multiple scattering events. This fluctuating field can be expressed in terms of the average field  $\langle \mathbf{E}_j \rangle$  at the position of some arbitrary particle  $j$  by:

$$\langle \mathbf{E} \rangle = \mathbf{E}^0 + \int S_j \langle \mathbf{E}_j \rangle G(\mathbf{r}_j) d\mathbf{r}_j. \quad (2.15)$$

This approximation and method of averaging is limited however, and works well only in media with a small fractional volume of scatterers [11].

### 2.3.5 The Radiative Transfer Equation

Analytical models of multiple scattering become too complicated when working with media which consist of a random distribution of scattering centres. The radiative transfer model describes the propagation of light through tissue using fundamental electromagnetic theory. Tissue can be considered as a random medium with wave phenomena such as polarisation and interference, as well as particle properties such as inelastic collisions, being ignored. The basic assumption in radiative transfer theory is that only the flow of energy through the medium is considered. The radiative transfer equation (RTE):

$$\frac{1}{c} \frac{\partial I(\mathbf{r}, t, \mathbf{s})}{\partial t} + \mathbf{s} \cdot \nabla I(\mathbf{r}, t, \mathbf{s}) + (\mu_a + \mu_s) I(\mathbf{r}, t, \mathbf{s}) = \mu_s \int_{4\pi} f(\mathbf{s}, \mathbf{s}') I(\mathbf{r}, t, \mathbf{s}') d^2 \mathbf{s}' + q(\mathbf{r}, t, \mathbf{s}), \quad (2.16)$$

describes the change of energy radiance  $I(\mathbf{r}, t, \mathbf{s})$  at position  $\mathbf{r}$  in direction  $\mathbf{s}$ , with the parameters:

$c$	speed of light in the medium
$\mu_a$	the absorption coefficient
$\mu_s$	the scattering coefficient
$f(\mathbf{s}, \mathbf{s}')$	the phase function
$q(\mathbf{r}, t, \mathbf{s})$	the radiation source

The energy radiance  $I(\mathbf{r}, t, \mathbf{s})$  is the energy transfer per unit time per unit solid angle  $d^2\mathbf{s}$  through a unit area at position  $r$  and time  $t$ . Thus integrating  $I(\mathbf{r}, t, \mathbf{s})$  over all angles gives the flux  $\Gamma$  through a unit area  $\mathbf{n}$

$$\Gamma(r, t) = \int_{4\pi} I(r, t, \mathbf{s}) \mathbf{s} \cdot \mathbf{n} d^2\mathbf{s}. \quad (2.17)$$

The RTE is derived by considering the balance in radiant energy in an arbitrary volume element of tissue. It is a balance equation relating the change of the energy radiance in time (1st term) to a change in energy flow (2nd term), loss due to absorption and scattering (3rd term), gain due to scattering sources (4th term), and gain due to radiation sources (5th term). Exact solutions of the RTE can be found for cases with isotropic scattering in simple geometries. Otherwise, no general solutions exist, so further approximations need to be made or numerical methods applied to solve the equation [12].

## 2.4 Beer-Lambert Law

The Beer-Lambert law, in relation to this work, describes the relationship between the intensity of light transmitted through an absorbing sample and the number of absorbing species within that sample, as well as the path length through which the light must travel, i.e. the thickness of the sample. Using Figure 2.7 [9] this relationship can be described mathematically.

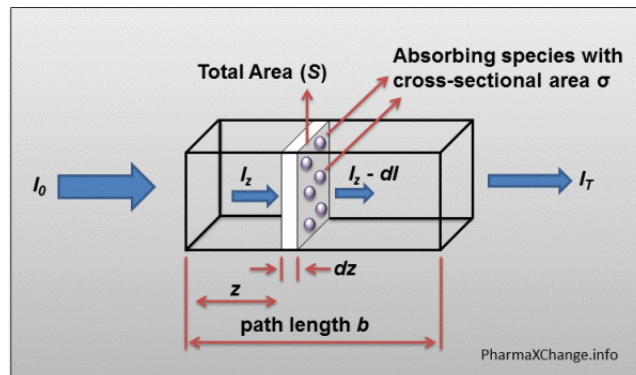


Figure 2.7: A diagram representing a sample of thickness  $b$  used for the derivation of the Beer-Lambert law [9]

Consider monochromatic light passing through the sample with incident intensity  $I_0$ , intensity upon entering the infinitesimal slab of thickness  $dz$  of  $I_z$  and transmitted intensity  $I_T$ . The absorption of photons through the path length  $b$  is due to the  $n$  molecules/cm<sup>3</sup>. The number of molecules present in the infinitesimal slab is hence:

$$n \times S \times dz,$$

and the total fractional area on the slab due to the absorbers is given by

$$(n \times S \times dz) \times (\sigma/S) = \sigma \times n \times dz,$$

since each absorbing molecule has area  $\sigma$ . Now, the light absorbed by the molecules in the infinitesimal slab is  $dI$  thus the fraction of light absorbed is given by  $dI/I_z$ . Since the total fractional area of the absorbing molecules is responsible for all of the absorption occurring in the slab, it follows that:

$$\begin{aligned} \frac{dI}{I_z} &= -\sigma \times n \times dz \\ \implies \int_0^b \frac{dI}{I_z} &= -\int_0^b \sigma \times n \times dz \\ \implies -\ln\left(\frac{I_z}{I_0}\right) &= \sigma \times n \times b, \end{aligned} \tag{2.18}$$

or, with a little manipulation, the expression above can be rewritten as

$$-\log\left(\frac{I_z}{I_0}\right) = A = \varepsilon \times b \times c, \tag{2.19}$$

where  $A$  is known as the absorbance,  $\varepsilon$  [M<sup>-1</sup>cm<sup>-1</sup>] is the wavelength-dependent molar absorptivity coefficient and  $c$  [M/l] is the absorber concentration [13]. This law can be readily applied to any medium that is purely absorbing. Tissue however, is a turbid medium and an absorption coefficient is not significant to understand light distribution within tissue. The Beer-Lambert law can still be applied to a fair degree of accuracy provided that the sample tissue minimises the number of scattering events, which roughly simulates a purely absorbing medium.

## 2.5 Light and Lasers in Biological Systems

### 2.5.1 Overview

When a laser beam is directed onto tissue, normally only 3% of the incident light is directly reflected [14]. The rest of the light travels into the tissue, where it can be either scattered, absorbed or transmitted. The rate at which heat is generated depends on the rate of absorption of photons within the tissue. For Nd:YAG lasers (1060 nm) and other lasers which have relatively high wavelengths, 30% to 50% of the incident light actually re-emerges from the tissue. When the absorptive capacity of a tissue is very high relative to its scattering ability, the laser beam remains strongly collimated in the tissue and the penetration depth becomes a function of the wavelength-dependent absorption coefficient. With wavelengths similar to that of an argon laser ( $\approx 500$  nm), the amount of absorption and scattering may be about the same in cardiovascular tissue [14]. In the red and infrared wavelength ranges, scattering is usually dominant. In general, blue light (460 nm) has a poor penetration depth as compared to red and near infrared wavelengths (650 to 1100 nm), which penetrates significantly deeper [14].

### 2.5.2 Characteristics and Properties of Biological Tissue

Tissue (in biology) is simply defined as a group or collection of cells that are similar in structure and function within an organism. A grouping of these tissues performing similar functions forms an organ, hence tissue is the intermediary between cells and a complete organ. The largest organ in the human body is the skin and it forms a large part of the focus of studies in biomedical science. Skin is multilayered and inhomogeneous, making it quite difficult to simulate [2].

The outermost layer of the skin is the stratum corneum and it is between 0.01 and 0.02 mm thick. It is sometimes considered part of the next layer of tissue, i.e. the epidermis. The stratum corneum does not absorb much light in the visible region of the spectrum and most incident light is transmitted. The epidermis is a structure, composed of four layers, with a total thickness

of between 0.027 and 0.15 mm. It typically absorbs light or transmits it (allows propagation), and the absorption is due to a natural pigment (chromophore) found in the epidermis, called melanin. There are two types of melanin, i.e. eumelanin (brown/black) and pheomelanin (red/yellow), both of which absorb a large range of frequencies, with greater absorption occurring at higher frequencies. Eumelanin is responsible for the skin colour of an individual and the ratio between the concentration of pheomelanin and eumelanin varies amongst individuals. Melanin is produced by cells called melanocytes which are found within thin membranes known as melanosomes. The amount of radiation that can be absorbed by melanin depends on the volume fraction of melanosomes in the epidermis [2].

The next structure is called the dermis and is approximately 0.6 - 3 mm thick and, like the epidermis, also primarily transmits and absorbs light. This layer of the skin contains the nerves and blood vessels, and is made up of dense and irregular connective tissue. The blood cells contain a chromophore called haemoglobin which absorbs light and gives blood its red colour. The two types of haemoglobin, oxygenated and deoxygenated absorb light slightly differently. Two other chromophores found in the dermis include bilirubin and  $\beta$ -carotene, which provide skin with its yellow/brownish colour [2].

The final layer is known as the hypodermis and is often not considered as part of the skin. It has varying sizes throughout the body. The hypodermis has a low absorption in the visible region, and can be up to 3 cm thick in the abdomen. This layer contains a number of white, fat cells which reflect most of the incident light back to the upper layers [2]. Figure 2.8 [6] indicates the hierarchy of tissue components by size.

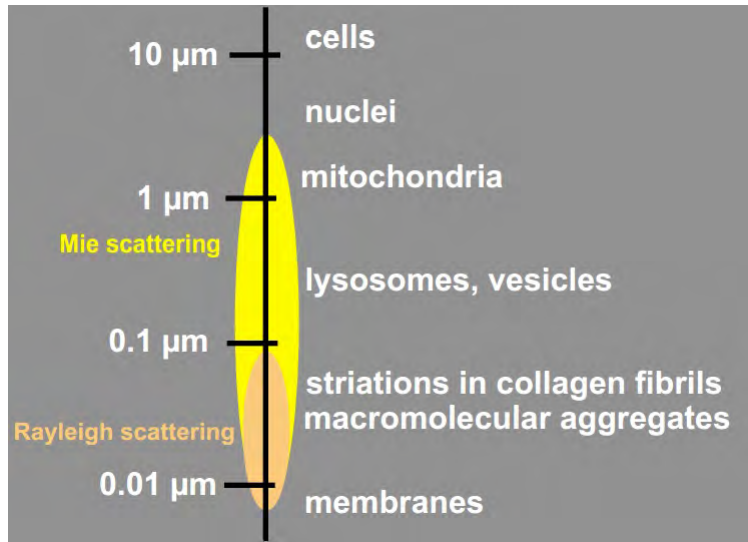


Figure 2.8: The relative sizes of various tissue components [6]

## 2.5.3 Light-Tissue Interactions

### 2.5.3.1 Propagation of Light in Tissue

The characteristics of tissue and the propagation of photons, which include scattering and absorption events within tissue, and reflection and transmission at boundaries, determine the number of photons that will reach the epidermis or dermis before being absorbed by a chromophore. Experimental evidence suggests that a large number of scattering events occur for each photon propagating through tissue, especially at visible and near infrared (IR) wavelengths. The mean distance travelled by a photon between scattering events is between 0.01 and 0.2 mm. At these wavelengths incident photons are more often scattered in the forward direction rather than the backward direction [15]. Most incident photons are never absorbed by the melanocyte, and besides being scattered, these photons can be absorbed by other chromophores in the tissue, totally internally reflected at the interface between air and tissue or even reflected out of the tissue. To exactly understand the propagation of light in tissue then would require modelling of the size and spatial distribution of the structures (absorbing and scattering) within the tissue, as well as their absorption and scattering properties. Tissue simu-

lation is clearly a difficult task and a simple way to represent tissue is to assume its base material to be largely absorbing, with a random distribution of scatterers within the volume of the sample. This sample would be isotropic and homogeneous over much of its volume, even though tissues in reality are not [15].

One of the main objectives of tissue optics is the formulation of methods to determine the absorbing and scattering characteristics of tissue. The optical properties to be discussed are all wavelength dependent and considered in the relevant human tissue. These properties are ideally determined non-invasively, which can be achieved with laser light, however, many of these properties are not known accurately as yet in the field of tissue optics. This is due to the result of changes that occur dynamically in tissue at different temperatures and water or oxygen concentrations, i.e. changes in the scattering and absorbing profiles of tissues [15].

### Transport Coefficients

Tissue is considered as a turbid medium, i.e. an incident photon is likely to undergo both scattering, in all directions, and absorption when incident upon a tissue. When a photon travels over an infinitesimal distance  $ds$  in tissue, the probability for scattering to occur over this infinitesimal distance is given by  $\mu_s ds$ , and similarly the probability of absorption occurring is  $\mu_a ds$ , where  $\mu_s$  and  $\mu_a$  are the coefficients of scattering and absorption respectively. The mean free path for an absorption event is  $\frac{1}{\mu_a}$  and for a scattering event is  $\frac{1}{\mu_s}$ . In a turbid medium it is conventional to describe the sum of the absorption and scattering coefficients, and this is known as the total attenuation coefficient or the transport coefficient  $\mu_t$  [15]:

$$\mu_t = \mu_a + \mu_s. \tag{2.20}$$

### Penetration Depth

The penetration depth  $\delta$  of a collimated beam is defined as the mean free path for an absorption or scattering event, i.e. the mean distance into the tissue that a photon from the incident beam will travel before it undergoes

scattering or absorption [15]. It is hence the reciprocal of the attenuation coefficient

$$\delta = \frac{1}{\mu_t}. \quad (2.21)$$

### Optical Depth

The optical depth  $OD$ , not to be confused with the physical depth  $d$ , is the product

$$OD = \mu_t d, \quad (2.22)$$

i.e. a greater optical depth means the photons travel a greater distance, on average, into the tissue.

### Albedo

The albedo  $a$  is defined as the ratio of the scattering coefficient to the transport coefficient

$$a = \frac{\mu_s}{\mu_t}. \quad (2.23)$$

For an optical albedo  $a = 0$ , the attenuation caused is by absorption only and for an albedo  $a = 1$ , only scattering occurs [15]. Figure 2.9 [16] depicts the albedo as a function of the scattering coefficient, with the absorption coefficient labeled as well.

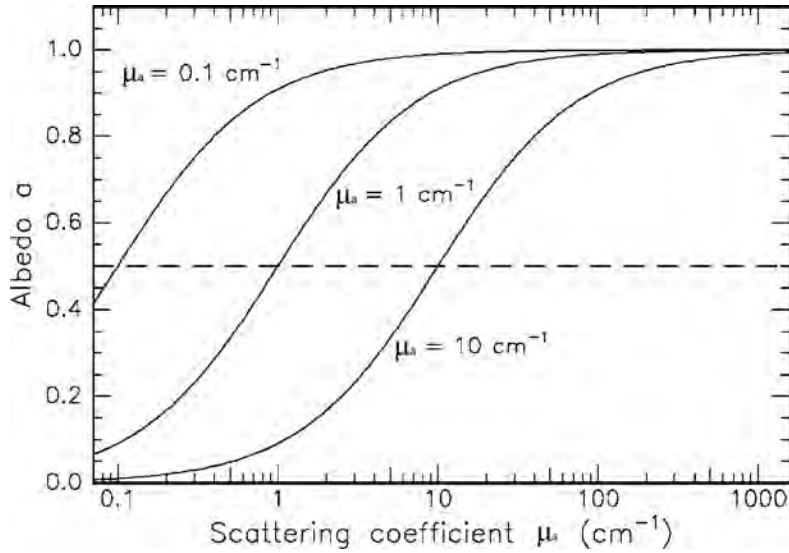


Figure 2.9: A graph of the optical albedo as a function of the scattering coefficient [16]

### Anisotropy

Light scattering in tissue is not isotropic and collimated light is scattered strongly in the forward direction. Measurements of the angular dispersion after scattering can be made using tissue samples thin enough to ensure that only a single scattering event will occur. The anisotropy factor  $g$  is the measure of the degree of anisotropy in a tissue, and represents the average scattering angle by that tissue [15], i.e.

$$g = \langle \cos \theta \rangle . \quad (2.24)$$

Total forward scattering means  $g = 1$ , total backscattering corresponds to  $g = -1$  and isotropic scattering implies that  $g = 0$ . The converse is not true for isotropic scattering however,  $g = 0$  does not necessarily indicate isotropic scattering [15]. Mie theory can be used to find analytical solutions for the phase function of plane electromagnetic waves by isotropic spherical particles of any size [12]. The anisotropy factor can then be expressed as

$$g = \langle \cos \theta \rangle = \int_{-1}^1 \cos \theta f(\cos \theta) d \cos \theta \quad (2.25)$$

Biological tissues generally scatter visible and near infrared light strongly in the forward direction with anisotropy factors in the range  $0.69 \leq g \leq 0.99$  [15]. The reduced scattering coefficient  $\mu_s'$  [ $\text{cm}^{-1}$ ] is defined as

$$\mu_s' = \mu_s(1 - g), \quad (2.26)$$

where  $1/\mu_s'$  is the mean path travelled by a collimated beam of light before it becomes isotropic [15]. Finally, the total transport coefficient  $\mu_t$  can be found from

$$\mu_t = \mu_s' + \mu_a = \mu_s(1 - g) + \mu_a. \quad (2.27)$$

### 2.5.3.2 Attenuation of Light

It is difficult to accurately measure the transmission of collimated light, in theory, as measurements of transmission are likely to include scattered light. Light that is transmitted through the air-tissue interface will undergo scattering or absorption at some point in the tissue. The absorption coefficient of melanin in tissue decreases as the wavelength of the incident light increases, whereas the absorption by blood depends on the wavelength and the oxygenation of the blood [15]. At certain wavelengths (known as isobestic points) the absorption of oxygenated and deoxygenated blood are equal, as shown by the points of intersection of Figure 2.10 [15].

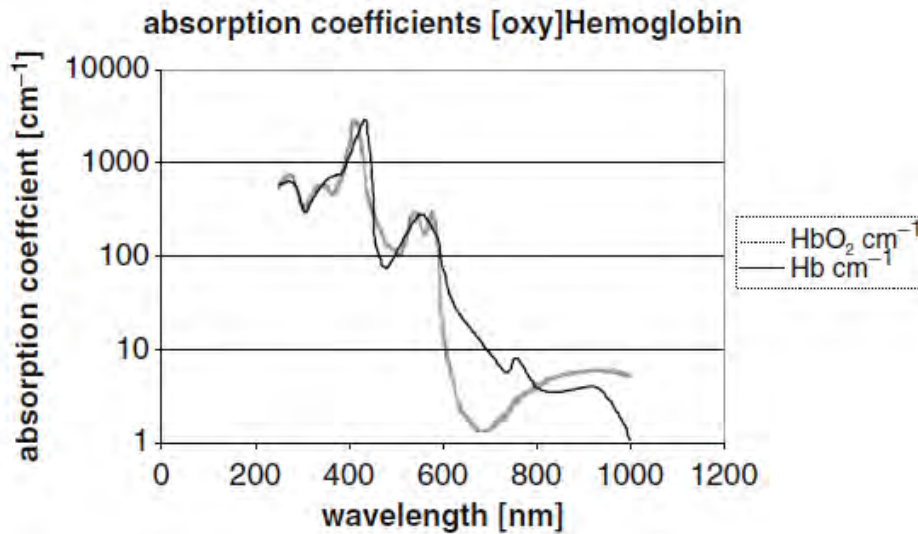


Figure 2.10: Absorption coefficient of oxy- and deoxyhaemoglobin as a function of wavelength [15]

Proteins and amino acids become the primary absorbers at wavelengths in the UV spectral range and water is the most highly absorbing of the chromophores at IR wavelengths. At wavelengths above that of  $1.4 \mu m$ , the scattering in tissue becomes insignificant as compared to the absorption. This wavelength is in the infrared range of the spectrum and hence the primary cause for attenuation in this range is water. The absorption coefficient (and hence the transport coefficient) of the tissue may then be estimated by the absorption coefficient of water, taking into account the concentration of water in that tissue. Changes in the temperature of water can also affect its absorption characteristics [15].

## 2.5.4 Photodynamic Therapy (PDT)

### 2.5.4.1 Lasers in Cancer Treatment

Three types of lasers currently being used to treat cancer are the CO<sub>2</sub>, Nd:YAG and the argon ion laser systems. The CO<sub>2</sub> laser is generally used to remove thin layers of tumours from the skin surface as it can cut and vaporize

tissue with little bleeding. It is often used to treat cancer in the vagina, cervix and vulva. The argon laser is used in conjunction with light sensitive drugs to kill cancerous cells. It can only penetrate a short distance into tissue, which makes it fairly ineffective in treating deeper tumours. The Nd:YAG laser can penetrate deeper into tissue and causes blood to clot quickly. It is often passed through thin, flexible tubes called endoscopes to reach nearly inaccessible areas deep within the body. It heats up the tumour directly and destroys it [17].

Lasers are also used to treat cancers of the intestine, oesophagus and bowel. They cannot cure these cancers completely, however they can lessen the severity of some of the symptoms and ease pain. The Nd:YAG laser is often used to treat cancer of the lungs and although it cannot completely destroy the tumour, it can aide breathing and prevent the patient from needing to undergo major surgery. In laser-induced interstitial thermotherapy (LITT), tumours are shrunk by depriving them of the things they need to survive, such as water and oxygen. Laser light is passed through fibre optic wires into a tumour where it heats it up and damages or destroys it. Lasers are powerful and precise which makes them ideally suited for cancer treatment and surgery. As technology improves, lasers should become a far more realistic and less invasive means of treating cancer, assuming doctors and surgeons are willing to adopt these methods and learn to use them effectively [17].

#### **2.5.4.2 Overview of PDT**

In PDT, a special drug called a photosensitising agent is added into the bloodstream. Over time it is absorbed by the tissues in the body. These chemical agents stay in and around cancerous tissue longer than they do normal tissue. The photosensitising agents are activated by irradiating the body with a certain frequency of light. This causes a chemical reaction to occur which kills cancerous cells. Light exposure has to therefore be carefully timed so as to allow the agent to leave healthy cells and surround the cancer cells. PDT is advantageous in that cancerous cells can be singled out and destroyed whilst healthy cells are spared. Also, the side effects of the photosensitising agents are generally fairly mild. However, the photosensitising agents, in some cases can leave people very sensitive to light, causing sunburn-like reactions after even brief exposure. The patient may have to

wait, sometimes for weeks, until the drug completely leaves the body. Argon laser light, generally used in PDT, however, cannot penetrate more than one centimetre of tissue, which means it is not very useful against deeper cancers [17].

PDT is sometimes used to treat pre-cancers and cancers of the oesophagus. Certain types of lung cancer can also be treated with PDT, using endoscopes. Researchers are currently looking at different kinds of lasers and photosensitising drugs that may be safer and more effective [17]. The photosensitisers used in PDT are usually activated by visible or near infrared light, which then allows specific biological effects to occur in cells or tissues. These biological effects can be utilised to treat certain types of tumours. The photosensitisers or the light used have no significant effect individually but the interaction of the two is effective. The interactions that occur between the light and tissue are photothermal and photomechanical in nature. PDT encompasses many various disciplines including physics, chemistry and biology [17].

#### 2.5.4.3 Mechanisms of PDT

The photosensitiser is initially in its ground state  $S_0$  and is excited to state  $S_1$  by the absorption of a photon of appropriate wavelength (as shown in Figure 2.12). It can then emit a photon of the same wavelength to return to state  $S_0$ , fluoresce or cross to a triplet energy state  $T_1$ . The  $T_1$  state is relatively longer lived ( $\sim \mu s$ ) than the  $S_1$  state since the transition from  $T_1$  to  $S_0$  is forbidden by quantum mechanics. In this time the triplet state can interact with the biological tissue in which the photosensitiser is located. This interaction can be directly with a biological molecule (type 1 interactions) or the  $T_1$  state can exchange energy with the ground state triplet molecule  $3CO_2$  (type 2 interactions). Type 2 interactions produce singlet  $O_2$  which reacts readily with biological molecules, has a lifetime of  $< 1 \mu s$  and diffuses through a distance  $\ll \mu m$  within the tissue [18]. The biological effect that results from the production of  $O_2$  is hence localised to the area in which the photosensitiser is introduced. The photosensitising agent will eventually regain its initial ground state and will either be destroyed directly by the interaction between light and the agent or indirectly through the dissolving of the  $O_2$ . Most photosensitisers that are currently used for PDT localise on cell membranes,

such as mitochondria and lysosomes. The limiting factor of this method is that a sufficient level of oxygen is required in the tissue for biological effects to occur, though most tumours have low levels of oxygenation. Figure 2.12 [18] shows the mechanisms of cell death in PDT.

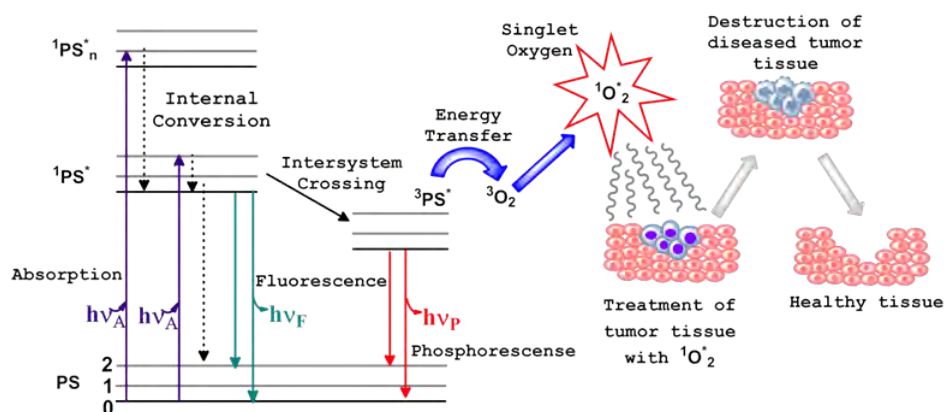


Figure 2.11: The electronic states and mechanism of cell death in PDT [18]

#### 2.5.4.4 Photosensitisers

Photosensitisers need to have a high absorption of a specific wavelength of photons that can penetrate to the required depth in tissue. They need also be highly localised to a tissue site to ensure biological effects occur only in the area requiring treatment and thus rapid removal of the agent is required, after treatment, to prevent patients from being left with photosensitivity. Some of the other considerations to be made are that the photosensitising agents need to be non-toxic, relatively simple to manufacture and cost effective. Different agents are used depending on the localisation of the tumour to be treated, and are chosen primarily according to their absorption spectra. Photofrin® is a drug used as a photosensitising agent in PDT that has a strong absorption for wavelengths around 400 nm and a much weaker absorption for photons of wavelengths around 630 nm. Since red light has greater penetration in tissues, a wavelength of around 630 nm is preferred in the treatment of tumours, even with its low absorption rate [19].

#### 2.5.4.5 Light

The energy required in PDT is large compared to that of radiation therapy. An absorbed dose in radiotherapy for solid tumours is approximately  $0.05 \text{ J cm}^{-3}$  whereas in PDT the average absorbed energy density can be  $\sim 100 \text{ J cm}^{-3}$ . Since light in the wavelength range applicable in PDT scatters or absorbs in a short distance through tissue, it becomes difficult to irradiate a sufficient volume of tissue at a significant depth. This scattering and absorption results in light becoming diffuse, sometimes within millimetres after passing through the tissue. The scattering in tissue decreases as the wavelength increases through the visible and near-infrared range and the absorption due to haemoglobin decreases rapidly at wavelengths above that of about 600 nm. The first absorption peak of water is reached at above 900 nm. It has been observed tissue necrosis occurs only in regions where the PDT product dose is above some threshold value and the effectiveness of the dose is proportional to the amount of light incident on the affected tissue, as the oxygenation and concentration of the agent can be kept constant [19].

#### 2.5.4.6 Action of PDT

The threshold concentration of  $\text{O}_2$  is obtained with a sufficient PDT dose, i.e. the combination of light, photosensitising agent and intrinsic oxygen. The  $\text{O}_2$  produced can either kill cells by necrosis (uncontrolled cell death) or by apoptosis (programmed cell death). PDT does not affect DNA significantly so the effects are direct rather than genetic, unlike radiotherapy or even certain drugs used in chemotherapy. Although there is a dependence on the type of photosensitiser used, the response of different cells to PDT is not largely varied. If the photosensitiser is present in cells lining blood vessels, these cells can be killed which can result in thrombus formation and cause blood flow in that region to cease. These effects along with others can lead to the death of that tissue. Cell death can trigger vascular responses in the body and even lead to vascular shutdown [19].

The majority of current PDT treatments are high dosage as compared to that of radiotherapy or chemotherapy, in which repeated small doses are given to the patient over time. Current PDT research is looking into applying this quantity of doses in the form of metronomic PDT (mPDT). In this treatment,

both the doses of light and photosensitizing agent are given in small doses repeatedly or continuously over a longer period of time. The aim of this method is to promote apoptosis to reduce the damage caused to healthy cells and tissues [19]. Figure 2.12 [19, p 243] shows some of the applications of PDT.

Application	Clinically approved (A) or under investigation (I)	Mechanism(s) of action
<i>Oncology:</i> solid tumors, dysplasias	A	cellular and/or vascular and/or possibly immunogenic
<i>Ophthalmology:</i> age related macular degeneration (AMD)	A	vascular
<i>Dermatology:</i> actinic keratosis psoriasis, acne, cosmesis	A I	cellular cellular and/or vascular
<i>Infection:</i> periodontitis, infected wounds, nail fungus blood purging	I I	cellular (microorganisms)
<i>Cardiology:</i> Prevention of restenosis	I	cellular and/or microvascular
<i>Rheumatology:</i> Arthritis	I	immunological and/or tissue destruction

Figure 2.12: Some of the current applications of PDT [19]

### 2.5.5 Measurement of Optical Properties of Tissue

It is important to measure different optical properties of a tissue in order to understand the structure and characteristics of that particular tissue. Direct measurements of the intensities of reflectance, transmittance and scattering are generally the primary measurements made and the absorption is inferred from these. It is difficult to measure absorption directly as the incident photons are "lost" in this process and knowledge of the incident intensity then allows for the calculation of the absorbed intensity. The total attenuation coefficient is easily measured as light propagates through the biological sample but the scattering and absorption coefficients can be measured depending on

the experimental technique used. The anisotropy factor can also be determined if the detector is rotated with respect to the sample, to measure the angular dependence of the scattered intensity [16].

Figure 2.13 [16] shows three typical setups for the measurement of the primary optical tissue properties. Fig. 2.13a represents the simplest arrangement which utilises a beamsplitter to obtain a reference signal on one detector (incident intensity) and the rest of the light is then allowed to pass through the sample. Another detector measures the transmitted intensity and the difference between the transmitted and incident intensities allows for the attenuation in the sample to be determined. Note that this setup does not allow for distinctions to be made between absorption and scattering, and only the total attenuation coefficient can be measured. Fig. 2.13b shows a setup in which the absorbance can be determined. An integrating sphere is used, within which the sample is placed, which has a highly reflective coating and a detector built in that only measures light that has not been absorbed by the sample. A measurement of the intensity is taken with and without the sample in place and the difference between these values is hence the intensity of light absorbed by the sample. The absorption coefficient can then be obtained with this information. In Fig. 2.13.c the detector rotates  $360^\circ$  around the sample and records the signal at different points of the rotation. The average scattering angle of the light through the tissue sample is measured in this way and subsequently used to calculate the anisotropy factor  $g$  [16].

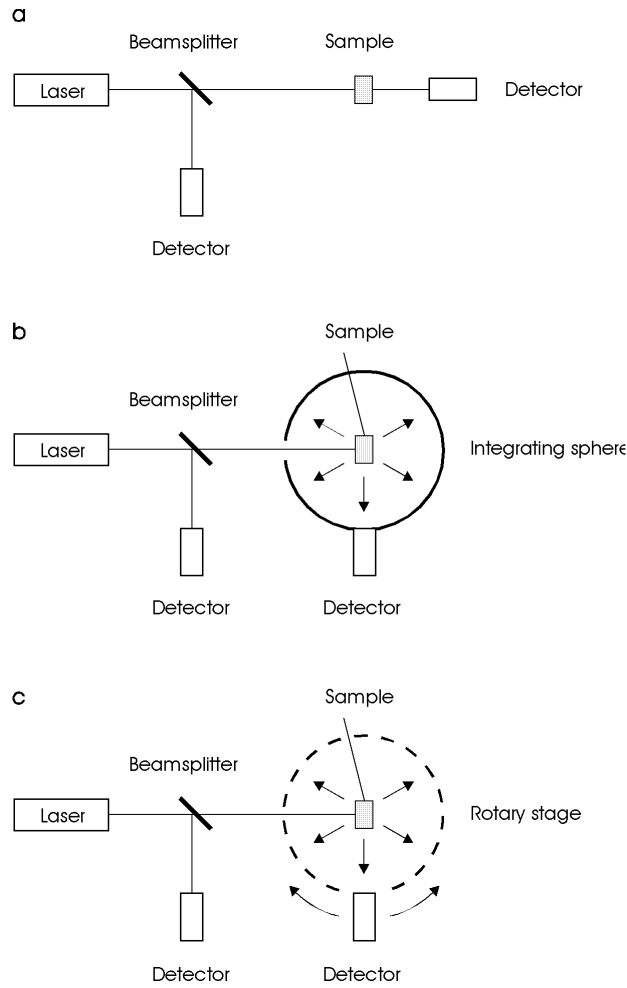


Figure 2.13: Experimental setups for measuring the total attenuation through a tissue sample [16]

One of the main disadvantages of the three techniques in Figure 2.13 is the fact that they cannot be carried out simultaneously. Since measurements of these optical properties affect the structure of the tissue itself unpredictably (e.g. tissue is heated by laser radiation), hence performing multiple experiments to measure all of the relevant properties has its drawbacks. A single sample may change over multiple experimental procedures and using many identical samples may yield completely different results each time. The best approach then is to measure all the important properties with a single ex-

perimental setup [16]. A double-integrating sphere can be applied to achieve this, via the use of two identical integrating spheres, one behind and the other in front of the sample. The sphere behind measures the intensity of incident radiation that is reflected at the air-tissue boundary or the intensity that is backscattered. The front sphere detects all transmitted and forward scattered light through the sample, hence all the important properties can be measured simultaneously. Kubelka-Munk theory is used to determine optical tissue properties with the introduction of coefficients for absorption and scattering. These Kubelka-Munk expressions work well for the propagation of light through tissue in one dimension, however biological tissue scatters light in three dimensions. Hence this method provides just a simple approximation of the propagation of light through tissue [16].

Absorption and scattering coefficients of tissue may vary during temperature changes, e.g. when incident upon by laser. Carbonization can lead to an increase in absorption whereas coagulation/condensing of tissues affects the amount of scattering. Figure 2.14 [16] shows the variation between the absorption and scattering coefficients of white matter in the human brain, in its normal and coagulated states. These properties were calculated using the Kubelka-Munk theory.

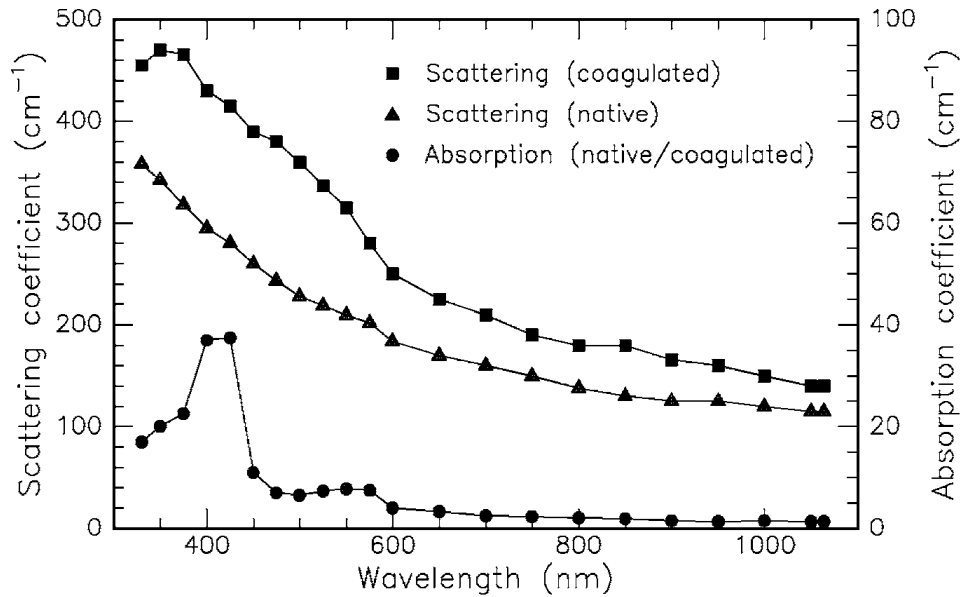


Figure 2.14: Optical properties of white matter of the human brain in its native and coagulated state [16]

Biological tissue is extremely inhomogeneous and the data obtained from two samples which may seem identical can vary significantly. Error bars can be quite large and are sometimes omitted in the study of tissue optics because of the large variation in results between experiments and theory. Slight alterations in the tissue can also vastly alter the properties of that tissue. A reliance of matching results with those that are published must be coupled with an understanding of the situation that is being considered in the setup and execution of the experiment, for relevant data to be obtained [16].

## 2.6 Tissue Phantoms

### 2.6.1 Overview

Determination of the optical properties of tissue is fundamental for application of light in either therapeutic or diagnostic procedures. A phantom tissue is a virtual or synthetic tissue created to simulate the optical properties and

model the transport of light in human tissue. The scattering and absorption coefficients, the anisotropy, etc. can be found for tissues in the human body from a well constructed simulating phantom. Phantoms can be also used to test the design, efficacy and setup of apparatus and calibrate equipment. In optical imaging, phantoms can be used to determine and compare the difference in polarization states of light, differentiate between different types of tissues and even detect tissue constituent concentrations [20]. The interaction between the components of a tissue phantom and incident light can be described with Mie theory, treating the scatterers in the medium as isolated, non-interacting spheres. The type of material used as well as their concentration in the creation of a phantom need to mimic the scattering and absorption characteristics of the tissue being simulated. Depending on the application, various scattering and absorbing materials in various concentrations can be combined to provide the required results. The base material in which the absorbers and scatterers are contained can be a solid or even a liquid [20]. Liquid phantoms are easy to produce as compared with solid phantoms, however solid phantoms are better suited to model tissues that are more complex in structure, e.g. multilayered tissue [21].

Techniques developed based on tissue models have been used to noninvasively monitor glucose and oxygenation in blood. Tissue-like phantoms are also extensively used in research connected with laser ablation, photothermal coagulation and PDT [4, 22]. The noninvasive nature of many biomedical procedures is, in some part, the result of work done on tissue simulating phantoms. It is of great interest to pursue this field of research since the diagnosis of medical conditions is best conducted noninvasively. One such diagnostic procedure is detecting breast cancer at an early stage by transillumination of light. It prevents the need for X-ray mammography which is potentially harmful. Breast tissue is highly scattering however and the technique had to be improved upon via the use of tissue phantoms, to simulate the multiple scattering in the breast. Many experiments are still being carried out on turbid media to try and determine the precise optical properties of the human breast in vivo [23]. Some of the methods used to determine the relevant optical properties of tissue include the use of an integrating sphere, frequency-domain diffuse reflectance, time domain diffuse-reflectance and optoacoustics among others [24]. The advantages and disadvantages differ between the techniques and the utilisation of the appropriate method

depends upon the situation or the specific geometry of the tissue being studied [24].

The optical properties of a tissue, once determined, can be used to predict light distribution and energy deposition on tissue. Many reviews in the past have found these optical properties *in vitro* and concluded that there exists uncertainty in this approach as living tissue of a particular person varies in blood and water content, etc. These are chromophores which will affect the attenuation in that tissue and variations in their levels have to be accounted for. It seems then more suitable to understand the behaviour of the optical tissue properties at the relevant wavelength than just the values of these coefficients themselves. The behaviour of tissue optical properties can be observed with the tissue's water, fat and blood content as controlled parameters. It is significantly more viable to adjust these parameters using tissue simulating materials than to attempt these experiments *in vivo* [25].

## **2.6.2 Discrete and Continuous Particle Models of Tissue**

### **2.6.2.1 Overview**

Tissues are generally composed of inhomogeneous structures with a wide range of sizes, randomly dispersed throughout the tissue medium. Tissue is regularly modelled as either a medium with a continuous random distribution of scattering and absorbing particles or as a discrete ensemble of scatterers and chromophores. The model used depends upon the structural complexity of the tissue being modelled or the extent of light scattering by that tissue. Blood is a good example of a biological system which fits the model in which the particles are discrete and dispersed. Most biological media are modelled as noninteracting, spherical particles since many cells and microorganisms are nearly spherical in shape, e.g. blood cells [26]. A system of noninteracting, spherical particles is the simplest model for tissue and hence Mie theory can be readily applied. Mie theory can be used to explain scattering by spherical particles, as well as cylindrical particles. Connective tissue and fibre structures can be modelled by approximating them to be long cylinders, and the scattering of these single homogeneous cylinders or even multilayered cylinders is understood using Mie theory [26].

### 2.6.2.2 Distribution of Scatterers

Cells and tissue structures vary from nanometres to hundreds of micrometres in size. Bacteria measure only a few micrometres in size. Erythrocytes, which are type of blood cell found in plasma are of the shape of a concave-concave disk with diameter approximately between 7.1 and 9.2  $\mu m$ , and a volume of 90  $\mu m^3$ . Leukocytes are nearly spherical in shape with a diameter of 8 to 22  $\mu m$  and platelets are convex-convex disk like particles with diameter in the range of 2 to 4  $\mu m$ . Fat cells can have a wide range of diameters from a few micrometres to around 75  $\mu m$  and in some cases reaching a diameter of 200  $\mu m$ . Other cell structures such as cell nuclei can be of the order 5 to 10  $\mu m$ , whereas structures such as ribosomes are much tinier with diameters of around 20 nm. All these structures contribute to the scattering of light through the tissue to varying degrees. Many of these scatterers are not perfectly spherical in shape and some can be modelled using ellipsoids. In fibrous tissues or tissues which have fibre layers, these elements can be approximated by cylinders with diameters between 10 and 400 nm and ranging from 10  $\mu m$  to a few millimetres in length [26]. In some tissues the distribution in sizes of the scattering particles is small whereas other tissues may have a broad variation in scatterer size. No universal size function could therefore be applied to describe the sizes of particles in all tissues. To describe the scattering by particles of complex shape, the T-matrix method may be applied or irregularly shaped particles may be considered as aggregates of spherical particles [26].

### 2.6.2.3 Absorption and Refractive Index

Cell nuclei, melanin particles, cell organelles, tissue fibres and others are the structures that are responsible for most of the variations of refractive index within tissue. The law of Gladstone and Dale [26] can be used to determine the refractive index of the interstitial medium, the tissue and its components, which is related to the volume fraction of the tissue occupied by these components. The refractive index of a particle can be defined as the sum of the background index and the mean index variation, where the average background index is defined as the weighted average of the refractive indices of the cytoplasm, which is the ground substance of a cell, and the interstitial fluid. The refractive index of cytoplasm is 1.38 and averaged refractive index

of a cell is about 1.42 [26]

Absorption by tissues is almost negligibly small in the visible light region with only haemoglobin, melanin and some other chromophores absorbing little light in this region. In the infrared region, most of the absorption is due to water molecules in tissue and protein bands contribute mainly to the absorption at UV wavelengths since these inhomogeneous tissue structures have sizes that are smaller or comparable in size to visible and NIR wavelengths and relatively small refractive indices. They are hence considered as optically soft [26].

#### **2.6.2.4 Tissue Anisotropy**

Most biological tissues are optically anisotropic and birefringent (i.e. they have refractive indices which are dependent on the polarization and propagation direction of light). Tendon consists mostly of parallel, densely packed collagen fibers which run parallel to a single axis, making tendon highly birefringent as a tissue. The angle between the orientation of polarization of linearly polarized light and the tissue axis determines the effects of birefringence in that tissue. For systems with large diameter cylinders ( $\lambda \ll$  cylinder diameter), the birefringence goes to zero. Values for the birefringence of tendon, muscle, and skin are on the order of  $10^{-3}$  [26]. Birefringence of the skin and cartilage are not as uniformly distributed as in tendon in their amplitude and orientation, i.e. collagen fibres in skin and cartilage do not have uniform densities as tendon does. Also the distribution of collagen fibres is not as ordered. Polarization-sensitive optical coherence tomography (PS OCT) is a technique that allows for the precise measurement of birefringence in turbid tissues. Since many biological tissues exhibit intrinsic or form birefringence, PS OCT techniques are often applied in ophthalmology, dentistry and dermatology [26]. Changes in birefringence can indicate functional alterations in tissue, such as photothermal injury during laser surgery which changes the birefringence in subsurface tissue [26].

#### **2.6.2.5 Volume Fraction of Tissue Components**

The volume fraction or packing density refers to the fraction of the total tissue volume occupied by its constituent particles. The volume fraction of a tissue

sample or phantom influences the optical properties such as the anisotropy and refractive index [26]. The inference of the volume fraction of a tissue sample, such as a phantom, can be made from a thin slice of the sample. These results can be misleading though as the distribution of scatterers are likely to be completely random throughout the sample [26]. Hence, the use of a different slice may result in an entirely different result being found. The volume fraction of scatterers in human tissue such as muscle and the cornea can range between 20 and 40%. In a cubic millimetre of blood, there exists  $(4-5)\times 10^6$  erythrocytes,  $(4-9)\times 10^3$  leukocytes and  $(2-3)\times 10^5$  platelets. 60% of blood is mostly plasma (composed of primarily water) whilst the rest is occupied by erythrocytes. At very small volume fractions of spherical particles suspended in solution, incoherent scattering occurs by independent particles, rather than coherent scattering which is observed with a large concentration of particles. In tissue the organization of particles is such that there are spaces between scattering particles comparable to their size [26].

## 2.6.3 Construction of Tissue Phantoms

### 2.6.3.1 Overview

A typical phantom consists of a host medium/diluent, a scattering medium and an absorbing medium. The goal is to form a mixture of the correct amounts of diluent, absorbers and scatterers to simulate the optical properties of the desired tissue. The properties that can be determined by measurements on the phantoms include the scattering coefficient  $\mu_s$ , the absorption coefficient  $\mu_a$  and the anisotropy  $g$ , among others. For soft tissues, typical ranges for these optical properties are  $\mu_a \in [0.5 ; 5.0] \text{ cm}^{-1}$ ,  $\mu_s \in [0.2 ; 400] \text{ cm}^{-1}$  and  $g=0.9$  for both visible and NIR wavelengths. Solid phantoms are generally made from transparent hosts, such as gelatin, agar or even wax which inherently scatter light. The simulation of tissues with complex geometries can be achieved by creating layered phantoms and inserting the inhomogeneities at the relevant sites. Multilayered phantoms describe tissues the best, however have proved to be complicated to create. These phantoms have to replicate the optical properties found in tissue at the desired wavelengths, but some tissue phantoms have realistic properties over a large range of wavelengths [4].

According to Tuchin [4], a realistic tissue phantom should satisfy the following requirements:

- It should model the geometry and optical parameters of the tissue that are relevant for the transport of light [4].
- All components of the phantom must be compatible with each other with regards to chemical stability and spectroscopic properties [4].
- The relevant parameters of radiation transport must be reproducible and predictable from the sample composition [4].
- The physical parameters of the phantom must be temporally stable (evaporation, diffusion, aging) and independent of environmental influence [4].
- The construction of the phantom should allow for inhomogeneous tissue geometries to be modelled by stacking phantom slabs or moulding techniques [4].
- The sample should be simple, quick and safe to prepare [4].

Realistic values for the optical properties of tissue over a broad range of wavelengths is achieved on the basis of the discrete particle tissue model. Mie theory can then be applied to determine the absorption and scattering by the particles in the tissue [4]. Some of the relevant parameters of the particles required for the application of Mie theory include the complex refractive index

$$n_s(\lambda_0) = n'_s(\lambda_0) + in''_s(\lambda_0), \quad (2.28)$$

the refractive index of the host material  $n_0$  and the relative refractive index of the scatterers and host  $m = \frac{n_s}{n_0}$ , where  $\lambda_0$  is the wavelength in vacuum and the imaginary part of the complex refractive index is responsible for the losses in light due to absorption. The scattering and absorption coefficients can also be found by the use of Ricatti-Bessel functions [4] in expressions for the Mie coefficients.

The mean distance  $d_s$  between scattering particles can be expressed in terms of the dimensionless volume fraction of scatterers  $c_s$  and the radius of scatterers  $a_s$  by

$$d_s = \frac{2a_s}{\sqrt[3]{c_s}} \quad (2.29)$$

Mie theory works best with regularly shaped particles, such as spheres and if the scattering particles have radius on the same order of magnitude as the incident light [4]. This is generally the case with materials used for the creation of tissue phantoms.

Shorter wavelengths are more likely to be scattered in biological tissue, with a high anisotropy. It is best then, to prepare a mixture of large particles which contribute a high anisotropy and small particles which scatter shorter wavelengths to accurately simulate biological tissue [4].

### 2.6.3.2 Host Media

Some of the phantom matrix options that can be used to hold the scatterers and absorbers include:

- aqueous solutions
- gel/agar matrix
- polyacrylamide gel
- polyester/polyurethane resin
- room temperature vulcanizing silicone

### 2.6.3.3 Scattering Media

In the manufacture of liquid phantoms the most common scattering materials are intravenous fat emulsions such as Intralipid, Nutralipid and Liposyn. These drugs contain soybean oil, egg phospholipids and glycerol and represent spherical fat droplets suspended in water. Intralipid based solid phantoms undergo a large variation in the scattering coefficient through a small change

in scatterer concentration. It has also been found that temperature changes during the production of solid phantoms could affect the structure of the scatterers and induce interactions with agar (typical ground material) [27].

Scatterers frequently used in the construction of solid tissue phantoms include polystyrene latex spheres, with a diameter on the order of a few micrometres.  $\text{TiO}_2$  and  $\text{Al}_2\text{O}_3$  particles which are spherical and range from 20 to 70 nm in diameter are also commonly used as a suspension in an aqueous or gel solution to scatter light. Quartz glass microspheres are more difficult to obtain but these particles can act as scatterers with diameter of around 250 nm. Polystyrene,  $\text{TiO}_2$  and  $\text{Al}_2\text{O}_3$  are hydrophilic in nature (do not dissolve in water) which make them ideal for use in solid phantoms with a base material of agar or gelatin. Sonication is generally carried out on warm gels to which scattering particles are added to prevent sedimentation of particles whilst the host material is still nonviscous (i.e. before the gel solidifies) [27].

#### **2.6.3.4 Absorbing Media**

Light absorption in tissue is modelled based on the absorption coefficient, which can be determined directly and indirectly in phantoms. Certain dyes are widely used as absorbing media in phantoms depending on their absorbances at different wavelengths and their solubility in the host material. Common stains used in microscopy absorb light in the visible and NIR spectral regions, ideal for the use in tissue-like simulations. Indocyanine green has often been used as an absorber for NIR wavelengths in gel based multilayered phantoms. Another vastly utilised absorbing medium is black India ink which is used as a common absorber in the visible region. Certain fluorophores can serve as absorbers in tissue phantoms as well [27].

# Chapter 3

## Experimental Details

### 3.1 Methodology

#### 3.1.1 Apparatus

The experimental setup used in this work is shown in Figure 3.1

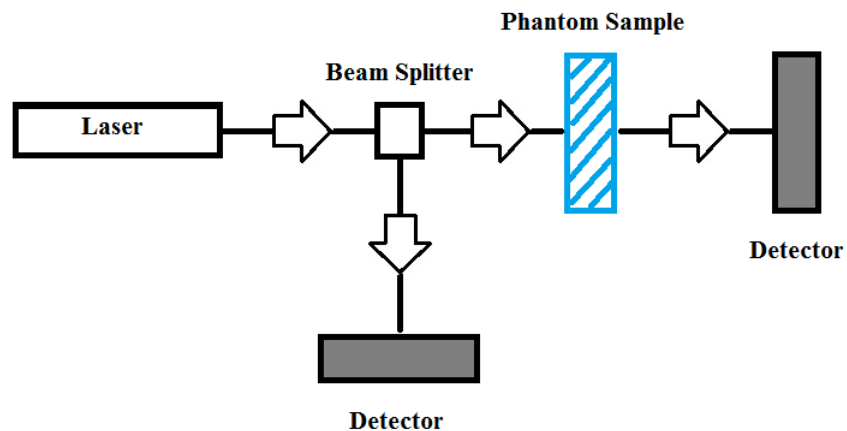


Figure 3.1: A diagram of the setup of apparatus for this experiment

An He-Ne red laser of wavelength 632.8 nm provided the collimated beam initially, but was replaced by an He-Ne 532 nm green laser for all subsequent

measurements. This was due to restrictions on the equipment available for use during the course of the work. Bacteriological agar powder was used as the base material for the phantom samples. The agar was mixed with deionised water and the mixture was then heated on a hot plate to the required temperature for activation of the agar. The temperature of the sample during the heating process was monitored using either a red alcohol thermometer or a Techgear TG732TK dual channel digital thermometer which had been modified to utilise a thermocouple attached on the reverse side of a velcro strap. The digital thermometer strap was attached around the outside of the beaker during heating and measured temperature of the solution in the beaker on an accuracy of  $\pm 5^{\circ}\text{C}$ . The samples were created within a standard 7 cm diameter glass beaker with high temperature capabilities. Black stamp pad ink was used to absorb the visible wavelengths of light used in this experiment whilst neutral  $\text{Al}_2\text{O}_3$  powder, which consists of tiny, roughly spherical particles served as the scatterer. The amount of scatterer and absorber used was determined with a digital balance (with a readability of 0.01 g) which was capable of measuring the relatively small masses of these materials accurately. The incident beam was split in two by a EO 47009 (Edmund Optics), 25 mm cube beam splitter and the power incident on and transmitted through the sample was measured with an EO 54-018 (Edmund Optics) digital handheld laser power meter.

Samples that were created were placed in a refrigerator, in a beaker covered with aluminium foil, overnight to solidify. To work within budget, slices of the sample were cut carefully, by hand, using a Stanley knife and their thicknesses measured via a set of digital vernier calipers. Care was taken to ensure that the integrity of the sample was kept intact throughout the slicing and measuring process.

### 3.1.2 Phantom Recipe

The recipe to create the phantom samples was similar to that used by Hartleb [30] as it was simple to prepare, requiring only readily available and inexpensive equipment:

1. A mixture comprising of 1.5 g of agar for every 100 ml of deionised water was prepared.

2. The mixture was heated to around 94°C on the hotplate. This being the temperature at which the agar activates.
3. The mixture was continuously stirred to allow all the granules of agar powder to dissolve.
4. The mixture was allowed to cool to around 70°C before the scatterers and/or absorbers were added.
5. The new mixture was again continuously stirred until it cooled sufficiently that the scatterers were suspended in solution (i.e. no sedimentation occurs).
6. The sample was placed in a refrigerator to solidify overnight.
7. Upon solidification, the agar forms a relatively firm gel (Figure 3.2).



Figure 3.2: A pure agar sample after solidification

It is important for the sample to be allowed to cool sufficiently before stirring can cease. This usually takes around 2 hours after the heating has ended. Even a sample at around 35°C can be nonviscous enough that the scattering  $\text{Al}_2\text{O}_3$  particles tend to sink to the bottom of the beaker. Once the sample has

cooled significantly the gel nature of the agar becomes more pronounced and the  $\text{Al}_2\text{O}_3$  particles suspend in the solution to provide an even distribution of scatterers throughout the sample. Figure 3.3 shows the difference between slices of samples, one of which has been stirred sufficiently until cool and the other has not. Sedimentation is clearly evident in the unstirred sample, i.e. an even distribution of scatterers is not evident in the unstirred sample.



Figure 3.3: An agar sample, containing  $\text{Al}_2\text{O}_3$  particles, which has been stirred sufficiently until cool (left) compared to one that has had sedimentation occurring (right)

### 3.1.3 Procedure

After each sample was fabricated, it was then sliced by hand into as thin slices as possible of varying thicknesses. The comparison between the transmitted and incident power of light through each slice was sought to understand the attenuation through the sample and to verify if the sample was a good optical simulation of biological tissue. From the Beer-Lambert law

$$\begin{aligned}\mu_t &= \mu_a + \mu_s \\ &= -\frac{1}{L} \ln \left( \frac{P}{P_0} \right)\end{aligned}\tag{3.1}$$

where  $L$  is the sample thickness,  $P_0$  is the power of the unattenuated beam and  $P$  is the power of transmitted light. For any absorption or scattering (neglecting reflection at the air-tissue surface) events that occur, the

power/intensity of light transmitted would be less than that which is incident. The Beer-Lambert law was applied in this work by assuming multiple scattering does not take place and that the scattering is caused by regular shaped spherical  $\text{Al}_2\text{O}_3$  particles. The laser beam was passed through each slice and the power incident on and transmitted through each slice was measured (in mW) using the laser power meter. For slices of varying thicknesses, the attenuation coefficient was measured and averaged out over all the slices from a single sample.

For a pure agar sample, the assumption

$$\mu_t \approx \mu_s \quad (3.2)$$

is made, since agar is a base material that has mainly intrinsic scattering properties and hence its absorption coefficient is much smaller than its scattering coefficient [28]. For a sample with both ink and  $\text{Al}_2\text{O}_3$  particles, it is impossible to differentiate, from this experimental setup, between the contributions from scattering and absorption individually. The best approach then was to create separate samples with just scatterers or absorbers to determine those coefficients independently and then a sample with both to measure the total attenuation coefficient. Using a setup similar to that in Figure 2.13a also means that the anisotropy was ignored in this experiment as the required apparatus to measure the anisotropy factor was not available. Measurements of the transport coefficients also allowed for the determination of the penetration depth  $\delta$  and albedo  $a$ . These results were then compared to those from other sources to determine if the creation of a simple, low cost phantom provides a viable optical simulation of biological tissue. Figure 3.4 is that of a complete tissue phantom with India ink as an absorber added with the scattering  $\text{Al}_2\text{O}_3$  particles in the agar gel mixture. The bubbles which are created during the process of the activation of agar are clearly visible once the gel has become solid and is one of the sources of the intrinsic scattering of agar.



Figure 3.4: A complete phantom sample with black India ink and  $\text{Al}_2\text{O}_3$  particles in the agar gel mixture

## 3.2 Results

### 3.2.1 Measurements

The first set of measurements were conducted using a red laser ( $\approx 5\text{mW}$ ) of wavelength 632.8 nm and all the subsequent measurements were carried out in the same manner, with a different laser. The thickness of each slice of the sample was measured by pouring different volumes of the gel into different beakers. This method was difficult and time consuming since the samples were extremely hot when nonviscous enough to be poured and some sedimentation and uneven distribution of scatterers occurred. The samples following this were sliced by hand to the appropriate thicknesses. The transport coefficient  $\mu_t = \mu_s^{agar}$  was calculated using equation 3.1.

Sample Thickness $L$ (mm)	Incident Power $P_0$ (mW)	Transmitted Power $P(L)$ (mW)	$\ln(P)$	Transport Coefficient $\mu_t = \mu_s^{agar}$ ( $\text{cm}^{-1}$ )
8.50	5.11	2.79	1.026	0.712
13.50	4.98	2.27	0.820	0.582
15.50	4.78	1.72	0.542	0.659
18.00	4.51	1.10	0.095	0.784
25.50	4.83	0.92	-0.083	0.650
29.50	5.01	0.54	-0.616	0.755
$L^{avg} = 18.42$			$\ln(P)^{avg} = 0.297$	$\mu_s^{avg} = 0.690$

Table 3.1: Measurements of the incident and transmitted power of a 632.8 nm wavelength, collimated light source through a pure agar sample, made with 100 ml of water and 1.5 g of agar, to determine the scattering coefficient of agar at this wavelength

A sample calculation, for the first measurement, from equation 3.1 for Table 3.1

$$\begin{aligned}
 \mu_t &= -\frac{1}{L} \ln\left(\frac{P}{P_0}\right) \\
 &= -\frac{1}{0.850} \ln\left(\frac{2.79}{5.11}\right) \\
 &= 0.712 \text{ cm}^{-1}
 \end{aligned}$$

All measurements conducted hereafter were done with the use of a 532 nm wavelength green laser ( $\approx 50$  mW) and the slices of the samples were cut by hand. The set of results in Table 3.2 are analogous to those in Table 3.1 with the only differences being the laser, and consequently a small difference in transport coefficients (wavelength dependence).

Sample Thickness $L$ (mm)	Incident Power $P_0$ (mW)	Transmitted Power $P(L)$ (mW)	$-\ln\left(\frac{P}{P_0}\right)$	Transport Coefficient $\mu_t = \mu_s^{agar}$ (cm <sup>-1</sup> )
2.48	24.6	22.1	0.107	0.432
3.34	25.3	21.7	0.153	0.460
5.58	27.8	20.3	0.314	0.563
7.62	32.4	20.1	0.477	0.627
11.32	32.5	17.7	0.608	0.537
$L^{avg} = 6.07$			avg= 0.332	$\mu_s^{avg} = 0.524$

Table 3.2: Measurements of the incident and transmitted power through a pure agar sample made with 100 ml of water and 1.5 g of agar, using light of wavelength 532 nm, to determine the scattering coefficient of agar at this wavelength

Table 3.3 shows the results of a setup where 5 ml (5.50 g) of black ink was added to the same concentration of agar and water. The volume of the total solution was increased to 200 ml of water and 3.0 g of agar to make a larger sample, which was easier to cut. The ink acted as an absorber of the visible laser light, analogous to melanin in human skin tissue. The total transport coefficient was then used to identify the contribution of the absorption coefficient, since the scattering of this concentration of agar gel has been calculated.

Sample Thickness $L$ (mm)	Incident Power $P_0$ (mW)	Transmitted Power $P(L)$ (mW)	Transport Coefficient $\mu_t$ ( $\text{cm}^{-1}$ )
2.13	27.9	19.3	1.730
4.58	28.7	17.0	1.143
5.92	27.6	17.4	0.779
8.27	26.3	13.5	0.806
11.27	27.9	12.5	0.712
			$\mu_t^{avg} = 1.034$

Table 3.3: Measurements of the incident and transmitted power through an agar sample made with 200 ml of water, 3.0 g of agar and 5 ml (5.50 g) of black ink, using light of wavelength 532 nm, to determine the transport coefficient of ink in agar at this wavelength

The transport coefficient is evidently larger for the absorbing sample than that of the pure agar sample due to the added attenuation caused by absorption. The amount of ink added to the sample was then halved to 2.5 ml (2.76 g) to determine the new transport coefficient (Table 3.4).

Sample Thickness $L$ (mm)	Incident Power $P_0$ (mW)	Transmitted Power $P(L)$ (mW)	Transport Coefficient $\mu_t$ ( $\text{cm}^{-1}$ )
3.15	28.0	22.1	0.751
6.10	28.2	16.7	0.859
7.28	24.3	15.5	0.618
8.39	27.9	15.0	0.740
11.91	28.5	12.9	0.665
			$\mu_t^{avg} = 0.727$

Table 3.4: Measurements of the incident and transmitted power through an agar sample made with 200 ml of water, 3.0 g of agar and 2.5 ml (2.76 g) of black ink, using light of wavelength 532 nm, to determine the transport coefficient of ink in agar at this wavelength

Table 3.5 contains the results of a sample that contained 200 ml of water, 3.0 g of agar and 0.1 g of  $\text{Al}_2\text{O}_3$  powder. This was to determine the scattering

of  $\text{Al}_2\text{O}_3$  and agar together and hence the contribution to the scattering by the aluminium oxide particles.

Sample Thickness $L$ (mm)	Incident Power $P_0$ (mW)	Transmitted Power $P(L)$ (mW)	Transport Coefficient $\mu_t$ ( $\text{cm}^{-1}$ )
2.21	21.6	18.5	0.701
3.75	25.0	20.3	0.555
4.56	31.7	24.0	0.610
6.28	27.3	18.4	0.628
9.43	27.6	16.3	0.558
			$\mu_t^{avg} = 0.610$

Table 3.5: Measurements of the incident and transmitted power through an agar sample made with 200 ml of water, 3.0 g of agar and 0.1 g of  $\text{Al}_2\text{O}_3$ , using light of wavelength 532 nm, to determine the transport coefficient of  $\text{Al}_2\text{O}_3$  in agar at this wavelength

The next samples that were created were those of the "complete" phantoms, for the purposes of this work. These samples included the ink and  $\text{Al}_2\text{O}_3$  particles in solution but the transport coefficients would not necessarily be the sum of the transport coefficients of the individual materials in agar as found before. This is due to the errors that may arise in conducting the experiment but more so from the fact that light scattered initially by the  $\text{Al}_2\text{O}_3$  particles may later be absorbed without being transmitted through the sample. The first complete phantom was created with the same concentration of agar to water, as well as 0.10 g of  $\text{Al}_2\text{O}_3$  powder and 5 ml of ink (Table 3.6) and the second was similar (Table 3.7) with the amount of ink again halved to 2.5 ml.

Sample Thickness $L$ (mm)	Incident Power $P_0$ (mW)	Transmitted Power $P(L)$ (mW)	$-\ln\left(\frac{P}{P_0}\right)$	Transport Coefficient $\mu_t$ ( $\text{cm}^{-1}$ )
1.60	24.0	20.7	0.148	0.925
3.50	27.3	16.9	0.480	1.370
4.48	26.1	17.5	0.400	0.892
5.38	27.9	16.9	0.501	0.932
9.61	29.3	11.1	0.971	1.010
11.21	29.6	10.3	1.056	0.942
$L^{avg} = 5.96$			avg= 0.593	$\mu_t^{avg} = 1.012$

Table 3.6: Measurements of the incident and transmitted power through a complete phantom sample made with 200 ml of water, 3.0 g of agar and 5 ml (5.51 g) of black ink, using light of wavelength 532 nm, to determine the transport coefficient of ink and  $\text{Al}_2\text{O}_3$  in agar at this wavelength

Sample Thickness $L$ (mm)	Incident Power $P_0$ (mW)	Transmitted Power $P(L)$ (mW)	$-\ln\left(\frac{P}{P_0}\right)$	Transport Coefficient $\mu_t$ ( $\text{cm}^{-1}$ )
2.68	26.6	20.7	0.251	0.936
3.51	25.9	18.4	0.342	0.974
6.46	28.5	16.3	0.559	0.865
7.18	26.6	16.5	0.478	0.665
13.32	27.7	11.9	0.845	0.634
$L^{avg} = 6.63$			avg= 0.495	$\mu_t^{avg} = 0.815$

Table 3.7: Measurements of the incident and transmitted power through a complete phantom sample made with 200 ml of water, 3.0 g of agar and 2.5 ml (2.75 g) of black ink, using light of wavelength 532 nm, to determine the transport coefficient of ink and  $\text{Al}_2\text{O}_3$  in agar at this wavelength

It can be immediately seen from the results that the transport coefficients showed an increase with an increase in absorption in the samples, which is to be expected. Apart from direct calculation, these transport coefficients can be determined by plotting the graphs of  $\ln\left(\frac{P}{P_0}\right)$  vs  $L$  for each sample, which

will produce a straight line, according to equation 3.2,

$$-\mu_t L = \ln \left( \frac{P}{P_0} \right) \quad (3.3)$$

with slope of  $-\mu_t$ . These graphs were plotted to calculate values for  $\mu_t$  and compare them to the direct measurements. The graphs were plotted using Gnuplot and the fit function of Gnuplot was used to fit a straight line through the measured data points. The fit function provided values for the slope which were in the units of  $\text{mm}^{-1}$  and these were then converted to  $\text{cm}^{-1}$ . The best fit curves were plotted on the same set of axes as the direct measurement data to observe the deviation of the direct results from what is 'expected'.

The graphs of  $\ln \left( \frac{P}{P_0} \right)$  values against the thicknesses  $L$  of the slices of both of the complete phantom samples as well as the pure agar sample were plotted with their respective best fit straight lines (Figures 3.5-3.7). Figures 3.6 and 3.7 indicate a slight 'drop' in the transmitted intensities of light at 3.5 and 6.5 mm respectively which is likely to be due to error and not significant in this work. These three graphs were then plotted on the same set of axes to compare the attenuation due to each sample (Figure 3.8).

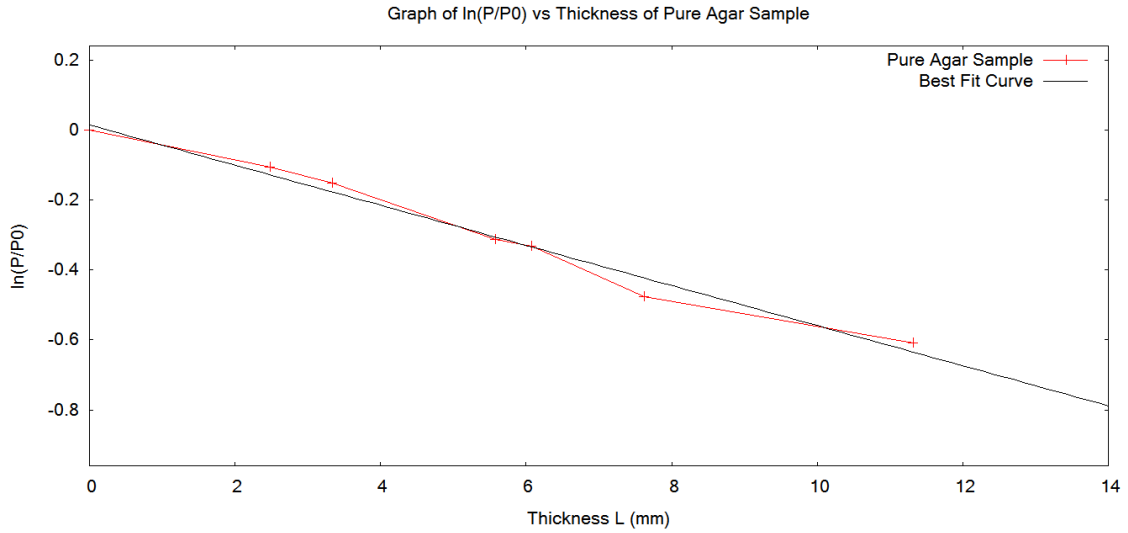


Figure 3.5: Graph of  $\ln\left(\frac{P}{P_0}\right)$  vs  $L$  for a pure agar sample with the associated best fit curve

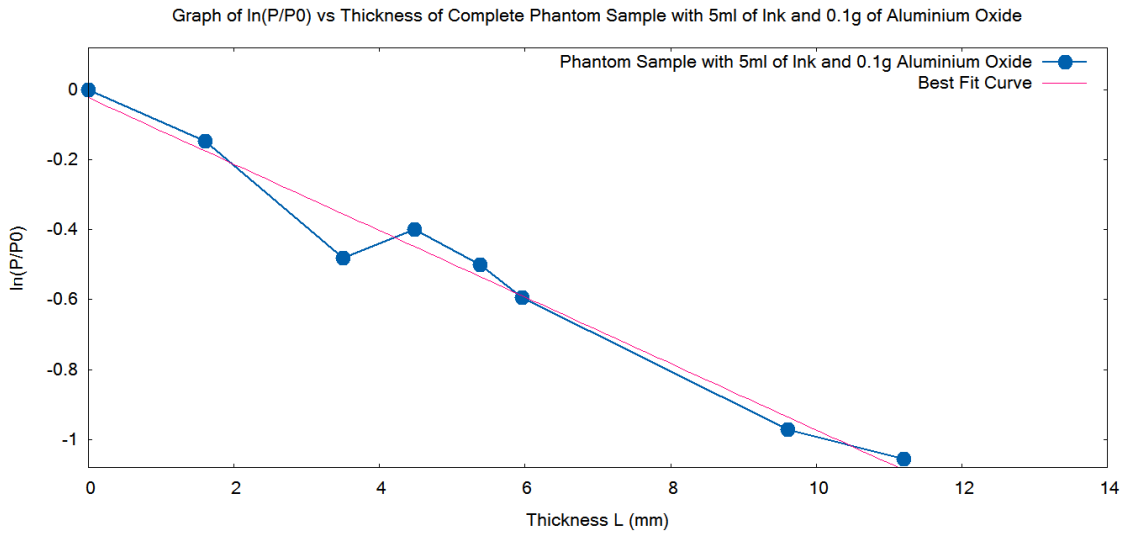


Figure 3.6: Graph of  $\ln\left(\frac{P}{P_0}\right)$  vs  $L$  for a complete phantom sample with 5 ml of ink and 0.10 g of  $\text{Al}_2\text{O}_3$ , with the associated best fit curve

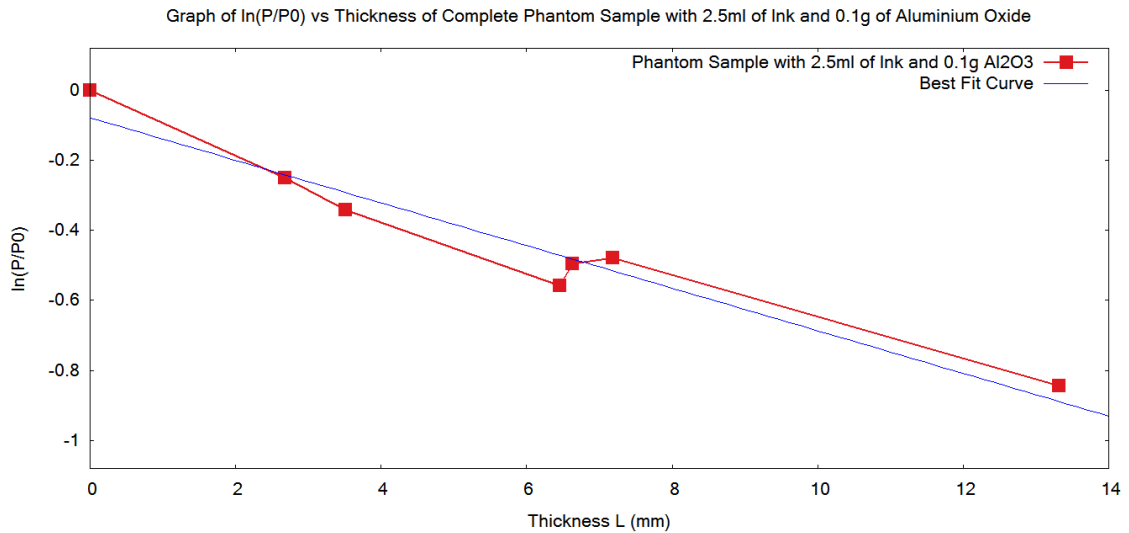


Figure 3.7: Graph of  $\ln\left(\frac{P}{P_0}\right)$  vs  $L$  for a complete phantom sample with 2.5 ml of ink and 0.10 g of  $\text{Al}_2\text{O}_3$ , with the associated best fit curve

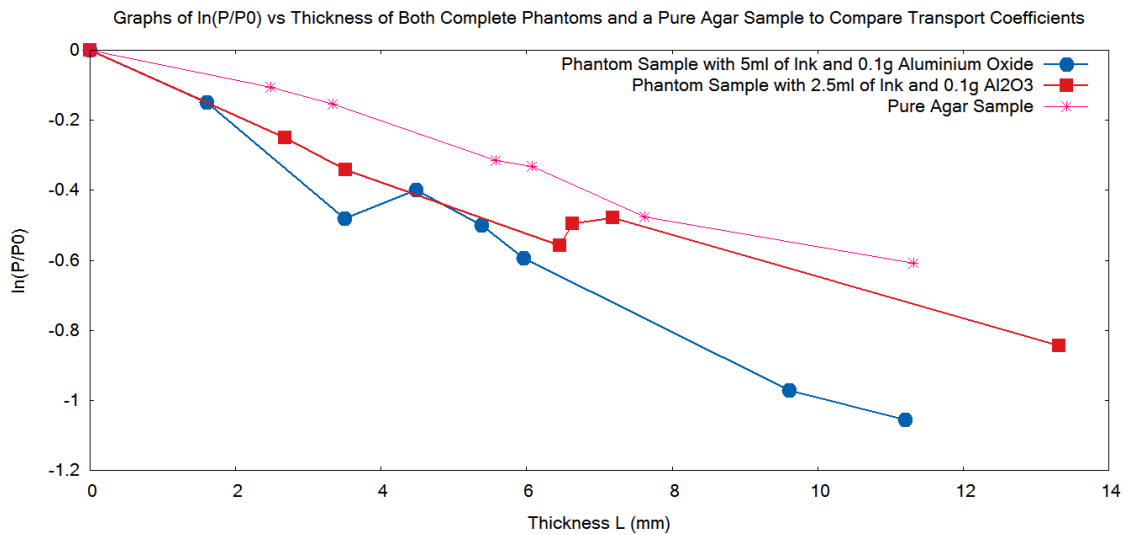


Figure 3.8: Graphs of all three samples plotted on the same set of axes to observe the difference in attenuation between samples

### 3.2.2 Analysis

Once these graphs had been plotted, the transport coefficients were determined by acquiring the slope of the best fit lines from Gnuplot. Table 3.8 shows the results obtained by calculation and Table 3.9 contains the results from Gnuplot, for each of the samples. The penetration depth  $\delta = \frac{1}{\mu_t}$  in each case was also calculated

Wavelength (nm)	Sample	$\mu_t(\text{cm}^{-1})$ [Calculation]	Penetration Depth $\delta$ (cm)
632.8	Pure agar	0.690	1.450
532.0	Pure agar	0.524	1.908
532.0	Agar with 0.1 g $\text{Al}_2\text{O}_3$ powder	0.610	1.639
532.0	Agar with 5 ml ink	1.034	0.967
532.0	Agar with 2.5 ml ink	0.727	1.376
532.0	Complete phantom with 5 ml ink and 0.1 g $\text{Al}_2\text{O}_3$	1.012	0.988
532.0	Complete phantom with 2.5 ml ink and 0.1 g $\text{Al}_2\text{O}_3$	0.815	1.227

Table 3.8: The transport coefficients and penetration depths for all the samples obtained by direct calculation

Wavelength (nm)	Sample	$\mu_t(\text{cm}^{-1})$ [Gnuplot]	Penetration Depth $\delta$ (cm)
532,0	Pure agar	0.573	1.745
532.0	Complete phantom with 5 ml ink and 0.1 g $\text{Al}_2\text{O}_3$	0.950	1.053
532.0	Complete phantom with 2.5 ml ink and 0.1 g $\text{Al}_2\text{O}_3$	0.608	1.645

Table 3.9: The transport coefficients and penetration depths for all the samples obtained from Gnuplot

From the analysis of the transport coefficients it is evident that  $\mu_t$  does not vary much between purely absorbing samples ( $\mu_t = 1.034 \text{ cm}^{-1}$ ) and the complete phantoms ( $\mu_t = 1.012 \text{ cm}^{-1}$ ) with  $\text{Al}_2\text{O}_3$  particles added. This indicates that the scattering due to these particles in the complete phantom is negligible which could be due to a few factors such as:

- errors in the measurements themselves
- sedimentation and uneven distribution of aluminium oxide particles, and
- absorption of scattered photons occurring.

The penetration depth  $\delta$  at 532 nm is greater in the pure agar sample than in the absorbing samples, a good indication that the ink used was an effective absorber at this wavelength. There is a small difference in transport coefficients between the pure agar sample and the agar sample with only the  $\text{Al}_2\text{O}_3$  scattering particles. The contribution therefore, of the  $\text{Al}_2\text{O}_3$  particles to the scattering is much less than the intrinsic scattering by the agar ( $\mu_s^{agar} \approx 0.5 \text{ cm}^{-1}$  and  $\mu_s^{Al_2O_3} \approx 0.1 \text{ cm}^{-1}$ ). It is not conclusive as to whether  $\text{Al}_2\text{O}_3$  is evidently not a strong scatterer at this wavelength or whether the scattering was just overshadowed by any absorption that would have happened after each possible scattering event in the complete phantom samples. The absorption

of the complete phantoms was the source of most of the attenuation, as well as the scattering due to the agar.

The complete phantom sample with 5 ml ink had a transport coefficient  $\mu_t \approx 1.0 \text{ cm}^{-1}$  and it was then possible to determine the absorption due to the 5 ml of ink

$$\begin{aligned}\mu_a^{5ml\text{ ink}} &= \mu_t^{5ml\text{ ink}} - \mu_s^{agar} \approx 1.0 - 0.5 \\ &= 0.5 \text{ cm}^{-1},\end{aligned}$$

and the optical albedo

$$\begin{aligned}a_1 &= \frac{\mu_s}{\mu_t} \\ &= 0.5.\end{aligned}$$

This represents an equal contribution by the scattering and absorption to the total attenuation through that sample. Similarly for the complete phantom sample that contained 2.5 ml of ink  $\mu_t \approx 0.8 \text{ cm}^{-1}$

$$\begin{aligned}\mu_a^{2.5ml\text{ ink}} &= \mu_t^{2.5ml\text{ ink}} - \mu_s^{agar} \approx 0.8 - 0.5 \\ &= 0.3 \text{ cm}^{-1},\end{aligned}$$

with an optical albedo

$$\begin{aligned}a_2 &= \frac{\mu_s}{\mu_t} \\ &= 0.625\end{aligned}$$

which indicates that 62.5% of the attenuation in this sample was due to scattering and hence 37.5% was caused by absorption. Therefore even small variations in the concentration of absorbers in the sample and similarly in tissue (with melanin) can greatly affect the albedo in that tissue.

Errors are difficult to treat in tissue optics since a single human tissue can display different optical characteristics at different times. Some of the sources of error include the intrinsic errors in the handheld power meter, including

its ability to only measure the power to three significant figures. The idea was also to create a homogenous sample each time with evenly distributed scatterers and absorbers which doesn't represent tissue in reality but is cheap and easy to create. Multilayered phantoms would be extremely difficult to create using agar, as the agar begins to slowly lose its structural integrity after even a few minutes at room temperature. During each measurement the sample had to be kept in the fridge as changes in its structure made it difficult to work with at times. Errors could also arise from the slicing of the sample, which is usually done by vibrotome to ensure slices of even thicknesses are cut. The measurement of each slice with a vibrotome is also far more accurate than the method used in this work. To test the experimental setup in a cost effective manner, all the materials and equipment were relatively cheap, easy to obtain and easy to use, but at the same time sufficient to provide meaningful results. Bacteriological agar is generally used to promote growth of bacterial cultures but can remain solid and usable for up to a month.

# Chapter 4

## Discussion

The results that were found proved to be reasonable and within the realm of acceptable values for the absorption coefficients in tissue optics. The values found for the attenuation coefficients ranged between  $0.3$  and  $1.0 \text{ cm}^{-1}$  which is relatively close to those in Table 4.1. Gebhart et al. [34] reported an absorption coefficient of  $0.6 - 0.9 \text{ cm}^{-1}$  for a similar wavelength range in the pons and thalamus. Salomatina et al. [38] found an absorption coefficient of  $0.6 \text{ cm}^{-1}$  at a wavelength of  $520 \text{ nm}$ , for the epidermis of caucasian skin. However, the measurements of scattering coefficients did not correlate with other results from theory. Table 4.1 shows values for the scattering coefficient being much larger than those observed in this work, e.g Salomatina et al. [38] found the scattering coefficient of the epidermis in caucasian skin to be  $6.51 \text{ cm}^{-1}$ . This value is much greater than any obtained in this work. Hence the phantoms created in this work would not serve as an accurate total representation of the epidermis in caucasian skin. Experimental results for the optical properties of most tissues vary widely but the measurements from different experiments place the values of each of the optical properties of a given tissue to within a certain order of magnitude. That is, there are no definite, theoretical values for the absorption coefficient, scattering coefficient, etc. but rather a range of acceptable values.

This work attempted to place the results within the range of acceptable values for as many of these optical properties as possible, without complicated methods or costly apparatus. It can be seen from table 4.1 that the values

for the absorption coefficient, at around the same wavelength, corresponded well with certain experimental results from human tissue.

$\lambda$ (nm)	$\mu_a$ ( $\text{cm}^{-1}$ )	$\mu_s$ ( $\text{cm}^{-1}$ )	Tissue	Source
633	1.4	88	bladder	Cheong et al. [29]
633	1.4	29.3	bladder	Splinter et al. [30]
514	1.3	190	bone (skull)	Roggan et al. [31]
665	1.3	1246	blood	Reynolds et al. [32]
630	1.4	473	grey matter	Yaroslavsky et al. [33]
630	1.5	386	white matter	
510	1.0	426	white matter (post mortem)	
500-600	0.6-0.9	109.4-133.7	pons	Gebhart et al. [34]
510-610	0.6-0.9	176.3-188.7	thalamus	
530	1.14	18.4	healthy tissue adjacent to invasive ductal carcinoma	Das, Liu, and Alfano [35]
550	1.1	18.48	dura mater (adult head)	Bashkatov [36] and Genina et al. [37]
520	0.6	6.51	epidermis (caucasian skin)	Salomatina et al. [38]
500	1.06	15.35	hypodermis	Paquit et al. [39]
550	0.67	11.4	Lyposyn plus blood	Kienle et al. [40]

Table 4.1: Optical properties of human tissue (in vitro) from various sources

Values for the absorption and scattering coefficients as well as other optical properties can be unique to certain tissues or even certain types of tumours, hence an understanding of the optical properties of a group of cancerous cells can allow further research to reveal the possibility of diagnosis and treatment of tumours in-vivo.

The values for the absorption coefficient obtained match closely to those of skin tissue, bone and even grey and white matter in the brain. The black ink provided an easy method to increase the absorption of the phantom sample. It is also easy to obtain and only a small quantity is needed to provide significant absorption of visible wavelengths. The scattering coefficients however are much larger than those obtained in this work. This cannot simply be adjusted by the addition of extra scatterers as this would lead to a dense packing of scattering centres in the phantom sample and the amount of  $\text{Al}_2\text{O}_3$  needed would be much greater than what was available. The remedy for this would possibly be to increase the size of the scatterers, eg. using  $\text{TiO}_2$  particles rather than the  $\text{Al}_2\text{O}_3$  particles that were used.  $\text{TiO}_2$  powder consists of larger, roughly spherical particles, more likely to scatter this wavelength of light. Polystyrene microspheres could also be a solution to the problem of insufficient scattering.

The accuracy and precision of the results could be improved by the use of a more sensitive power/intensity meter to allow for more significant figures in the calculation of absorption and scattering coefficients. The power of the laser light source was also seen to fluctuate by  $\pm 5$  mW during a single experimental procedure. This is around a 10% variation in the total power of the laser. The results could be greatly improved then with the use of a more powerful, stable laser light source. This however could drive up costs and would act against the aim of this experimental setup. An automatic stirrer, if cost effective, would provide much greater efficiency in the lab. A single sample had to be stirred by hand for more than an hour and a half before the solution solidified which is tiring and time-consuming. If left unattended while in aqueous gel form, some of the sample may solidify before the rest, leaving sediments (of the scatterers in the gel) clumped together rather than evenly distributed throughout the sample. This would consequently affect the scattering of the sample. The greatest difficulty in this experimental setup was the slicing of the sample. Agar in solid form is soft and tricky to work

with and this makes slicing by hand a difficult task to complete accurately. It is however the quickest and simplest method. The alternative would be to employ the use of a vibrotome which is a device that cuts thin slices of solid samples. The slices are accurately cut to the thickness desired and many more slices can hence be obtained without compromising the physical integrity of the sample. The drawback of this piece of equipment is that it is not readily available and extremely expensive to acquire.

# Chapter 5

## Conclusion

Altogether, the samples are relatively easy to create and work with and provide good results in terms of absorption of visible light. The scattering properties could likely be improved by the use of the microspheres mentioned. Many other particles that could in theory scatter visible light will dissolve in solution, which would negate the scattering effect and render them useless in this type of phantom. The ease of setup and the cost effective manner of acquiring materials and apparatus makes this an efficient method to utilise. The close correlation of the absorbing effects to those of human tissue is promising in the study of tissue optics. If a suitable scattering material could be found, and the experimental procedure ironed out, future work with this experimental setup would provide valuable data relating to tissue-like phantoms. This setup can be extended to include the use of an integrating sphere to find the anisotropy factor  $g$ . This in turn can be used to find the reduced coefficients of scattering and absorption which will lead to more accurate results. As is, the experimental setup is quick, repeatable, fairly reliable and produces good results in some aspects. The expectation and hope is that simple experimental setups such as this can become reliable enough to be of use in medicine and biology and allow for an easy tool for diagnostics, that can be implemented in little time, by anybody.

# Bibliography

- [1] Ghosh S, Soni J, Purwar H, et al. Differing Self-similarity in Light Scattering Spectra: A Potential Tool for Pre-cancer Detection. *Optical Society of America*. 2011; 1.
- [2] Baranoski GVG, Krishnaswamy A. *An Introduction to Light Interaction with Human Skin*. RITA. 2004.
- [3] Hutchison AM, Beard DJ, Bishop J, Pallister I, Davies W. An Investigation of the Transmission and Attenuation of Intense Pulsed Light on Samples of Human Achilles Tendon and Surrounding Tissue. *Lasers in Surgery and Medicine*. 2012; 44.
- [4] Tuchin VV. *Tissue Optics: Light Scattering Methods and Instruments for Medical Diagnosis*. 2nd ed. Bellingham: SPIE; 2007.
- [5] Taylor EF. *Illumination Fundamentals*. Rensselaer Polytechnic Institute. 2000.
- [6] Spectrophotometry. [found on the internet]. Available from [http://chemwiki.ucdavis.edu/Physical\\_Chemistry/Kinetics/Reaction\\_Rates/Experimental\\_Determination\\_of\\_Kinetics/Spectrophotometry](http://chemwiki.ucdavis.edu/Physical_Chemistry/Kinetics/Reaction_Rates/Experimental_Determination_of_Kinetics/Spectrophotometry).
- [7] Kim A, Keller JB. *Light Propagation in Biological Tissue*. Departments of Mathematics and Mechanical Engineering Stanford University, USA.
- [8] Sviridov A, Hassan VCM, Russo A, et al. Intensity Profiles of Linearly Polarized Light Backscattered from Skin and Tissue-like Phantoms. *Journal of Biomedical Optics*. 2005; 10(1).
- [9] Bass M. *Handbook of Optics Volume II: Devices, Measurements, and Properties* 2nd ed. United States of America: McGraw-Hill, inc. 1995.

- [10] Bass M. Handbook of Optics Volume I: Fundamentals, Techniques, and Design 2nd ed. United States of America: McGraw-Hill, inc. 1995.
- [11] Bass M. Handbook of Optics Volume III: Classical Optics, Vision Optics, X-ray Optics. 2nd ed. United States of America: McGraw-Hill, inc.
- [12] UCL Department of Medical Physics and Bioengineering. [found on the internet]. Available from [http://www.medphys.ucl.ac.uk/research/borl/homepages/florian/thesis/pdf\\_files/p45\\_58.pdf](http://www.medphys.ucl.ac.uk/research/borl/homepages/florian/thesis/pdf_files/p45_58.pdf).
- [13] College of Life Science, National Tsing Hua University. [found on the internet]. Available from <http://life.nthu.edu.tw/~labcyjw/BioPhyChem/Spectroscopy/beerslaw.htm>.
- [14] Welch AJ, Torres JH, Cheong W. Laser Physics and Laser-Tissue Interaction. Texas Heart Institute Journal. 1989; 16:141-9.
- [15] Welch AJ, van Gemert MJC. Optical-Thermal Response of Laser-Irradiated Tissue. 2nd ed. Springer. 2011.
- [16] Niemz MH. Laser-Tissue Interactions: Fundamentals and Applications. 3rd ed. Springer. 2007.
- [17] American Cancer Society [found on the internet] Available from <http://www.cancer.org/treatment/treatmentsandsideeffects/treatmenttypes/lasers-in-cancer-treatment>.
- [18] James NS, Ohulchanskyy TY, Chen Y, et al. Comparative Tumor Imaging and PDT Efficacy of HPPH Conjugated in the Mono- and Di-Forms to Various Polymethine Cyanine Dyes: Part - 2. Theranostics 2013; 3(9):703-718. [found on the internet]. Available from <http://www.thno.org/v03p0703.htm>.
- [19] Wilson BC, Tuchin VV, Tanev S. Advances in Biophotonics. (Eds.) IOS Press. 2005.
- [20] Avanaki MRN, Hojjat A, Podeleanu AG. Multilayer Tissue-Like Optical Phantom; a Model for Skin in Optical Coherence Tomography Imaging. Microscopy Focus. 2010.

- [21] Ayers F, Grant A, Kuo D, Cuccia DJ, Durkin AJ. Fabrication and Characterization of Silicone-based Tissue Phantoms with Tunable Optical Properties in the Visible and Near Infrared Domain. SPIE; 6870 687007-2.
- [22] Ramakrishna SA, Rao KD. Pramana Journal of Physics. Estimation of Light Transport Parameters in Biological Media using Coherent Backscattering. 2000; 54.
- [23] Mitic G, Wolfgang J, Kolzer Z, Otto J, Plies E, Solkner G. Time-gated Transillumination of Biological Tissues and Tissue-like Phantoms. Applied Optics. 1994; 38.
- [24] Koval G, Blair G, Jacques SL, et al. In Vivo Determination of Optical Properties of Normal and Tumor Tissue with White Light Reflectance and an Empirical Light Transport Model during Endoscopy. Journal of Biomedical Optics. 2005; 10(3).
- [25] Jacques SL. Optical Properties of Biological Tissues: A Review. Physics in Medicine and Biology. 2013; 58.
- [26] Tuchin VV, Zimnyakov DA, Wang LV. Optical Polarization in Biomedical Applications. Springer. 3rd ed. 2006.
- [27] Pravdin AB, Chernova SP, Papazoglou TG, Tuchin VV. Handbook of Optical Biomedical Diagnostics. Chapter 5: Tissue Phantoms. Bellingham: SPIE; 2002.
- [28] Hartleb C. Creation and Evaluation of Solid Optical Tissue Phantoms for Bio-medical Optics Applications. Ilmenau University of Technology. 2005.
- [29] Cheong WF, Motamedi M, Welch AJ. Optical Modeling of Laser Photocoagulation of Bladder Tissue. Lasers in Surgery and Medicine. 1987.
- [30] Splinter R, Cheong WF, van Gemert MJC, Welch AJ. In Vitro Optical Properties of Human and Canine Brain and Urinary Bladder Tissues at 633 nm. Lasers Surg. Med. 1989.
- [31] Roggan A, Albrecht H, Dorschel K, Minet O, Muller G. Experimental Set-up and Monte-Carlo Model for the Determination of Optical Tissue

- Properties in the Wavelength Range 330–1100 nm. Proc. SPIE 2323. 1995.
- [32] Reynolds LO, Johnson CC, Ishimaru A. Diffuse Reflectance from a Finite Blood Medium: Applications to the Modeling of Fiber Optic Catheters. Applied Optics. 1976.
  - [33] Yaroslavsky AN, Schulze PC, Yaroslavsky IV, Schober R, Ulrich F, Schwarzmaier HJ. Optical Properties of Selected Native and Coagulated Human Brain Tissues In Vitro in the Visible and Near Infrared Spectral Range. Physics in Medicine and Biology. 2002; 47.
  - [34] Gebhart SC, Lin WC, Mahadevan-Jansen A. In Vitro Determination of Normal and Neoplastic Human Brain Tissue Optical Properties Using Inverse Adding-Doubling. Phys. Med. Biol. 2006; 51.
  - [35] Das BB, Liu F, Alfano RR. Time-Resolved Fluorescence and Photon Migration Studies in Biomedical and Random Media. Rep. Prog. Phys. 1997; 60.
  - [36] Bashkatov AN. Controlling of Optical Properties of Tissues at Action by Osmotically Active Immersion Liquids. Cand. Science Thesis, Saratov State Univ. Saratov. 2002.
  - [37] Genina EA, Bashkatov AN, Kochubey VI, Tuchin VV. Optical Clearing of Human Dura Mater. Opt. Spectrosc. 2005; 98: No. 3.
  - [38] Salomatina E, Jiang B, Novak J, Yaroslavsky AN. Optical Properties of Normal and Cancerous Human Skin in the Visible and Near Infrared Spectral Range. J. Biomed. Opt. 2006.
  - [39] Paquit VC, M'eriaudeau F, Price JR, Tobin KW. Simulation of Skin Reflectance Images using 3D Tissue Modeling and Multispectral Monte Carlo Light Propagation. Conf Proc IEEE: Engineering in Medicine and Biology Society. 2008.
  - [40] Kienle A, Lilge L, Vitkin I, et al. Why Do Veins Appear Blue? A New Look at Old Question. Appl. Opt. 1996; 35: No. 7.